C.P. No. 508
(19,632)
A.R.C. Technical Report

C.P. No. 508
(19,632)
A.R.C. Technical Report





MINISTRY OF AVIATION

*AERONAUTICAL RESEARCH COUNCIL*

*CURRENT PAPERS*

# Preliminary Results of Low Speed Wind Tunnel Tests on a Gothic Wing of Aspect Ratio 1·0

*by*

*D. H. Peckham and S. A. Atkinson*

LONDON: HER MAJESTY'S STATIONERY OFFICE

1960

FIVE SHILLINGS NET

R21836

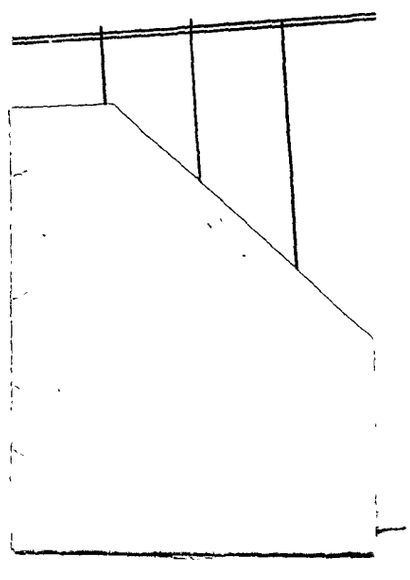

C.P. No. 508

U.D.C. No. 533.6.011.3: 533.691.13: 533.69.048.3: 532.527

Technical Note No. Aero.2504

April, 1957

ROYAL AIRCRAFT ESTABLISHMENT

# Preliminary results of low speed wind tunnel tests on a Gothic wing of aspect ratio 1.0

by

D. H. Peckham
and
S. A. Atkinson

---

## SUMMARY

This note gives preliminary results of low speed balance measurements and flow visualisation tests, on a wing of aspect ratio 1.0. The wing had a convex parabolic leading-edge shape in plan view, and an unswept trailing edge - such wings are now termed "Gothic". All edges were sharp, the centre section was 12% biconvex, and transverse sections were diamond-shaped.

Results of tests on a strictly comparable delta wing are not yet available, but where possible the results are compared with tests on other wings of aspect ratio 1.0 with unswept trailing edges.

---

## LIST OF CONTENTS



## LIST OF TABLES



## LIST OF ILLUSTRATIONS

## 1 Introduction

In a report by Weber[1] on the effects of flow separation on delta wings, cropped delta wings are briefly considered where the leading-edge and tip vortex sheets combine to give rather large non-linear lift increments and relatively low values of the drag due to lift. Comparing flat-plate wings of the same aspect ratio, it appears that a cropped-delta of taper ratio 0.5 has better lift characteristics at low speeds than a pure delta - at the expense of a loss in leading edge sweep. It was thought, however, that it might be advantageous for the development of the vortex sheets, to avoid the kinks in the edges and to have a curved planform in which the leading-edge and tip are faired to form one continuous curve. One then obtains a wing of steadily increasing leading-edge sweep with a "smooth" cross-section-area distribution. Such wings were, therefore, included in an investigation[2] of the geometrical properties of wings of small aspect ratio. The term "Gothic" wing has become popular in describing this planform shape.

A number of Gothic wings with a NACA 0012 round-leading-edge aerofoil section have been tested before at the suggestion of Voepel[3], and the results are summarised in Refs. 3 and 4. At low incidences the flow was mostly attached along the leading edge, but at higher incidences the flow began to separate along an appreciable part of the leading edge near the tips, this separation spreading inboard along the leading edge with increasing incidence to give a non-linear lift increase in the same manner as similar sharp-edged wings. Here also, using aspect ratio as a basis for comparison, it was found that the Gothic shape had better low speed lift characteristics than the corresponding delta, higher lift coefficients being obtained in the attached flow as well as in the separated flow regimes. Lift curves for the sharp-edged cropped delta and delta of Ref.1 are plotted in Fig.1(b), the curves for round-leading-edge Gothic and delta wings of Ref.4 being plotted in Fig.1(a).

A sharp-edged Gothic wing, of aspect ratio 1.0, has been included in a series of tests in the 13' × 9' low speed tunnel, to investigate the effects of planform taper and thickness taper on low aspect ratio wings at zero incidence as discussed in Ref.5. The wing was also tested over a large incidence and yaw range, in particular to investigate its lift and drag characteristics, and the behaviour of the separated flow. Although results of tests on a strictly comparable delta wing are not yet available, it is felt that the preliminary results are of sufficient interest to justify publication.

## 2 Description of models and tests

### 2.1 Description of models

The wing tested was of aspect ratio 1.0 and had a symmetrical biconvex parabolic arc section of 12% thickness/chord ratio at the root, and straight surface generators perpendicular to the wing centre line - giving diamond-shaped cross-sections. The leading edge planform was of parabolic shape, with the vertex at the tip. A drawing of the wing is given in Fig.2 and its geometry is discussed in Ref.2. The main model tested was of 16 $ft^2$ wing area, but brief tests were also made on a similar model of 4 $ft^2$ wing area to obtain information on interference effects from the tunnel walls.

If $c_o$ is the root chord, $t_o$ the root thickness, b the span, and if x is measured from the leading edge apex, the following relations apply:-

| | |
|---|---|
| Wing area, S | $= \frac{2}{3} bc_o$ |
| Aspect ratio, A | $= \frac{3}{2} \frac{b}{c_o}$ |
| Aerodynamic mean chord, $\bar{\bar{c}}$ | $= \frac{3}{4} c_o$ |
| Distance of mean $\frac{1}{4}$ - chord point from nose | $= \frac{7}{16} c_o$ |
| Wing cross-section area distance x from nose | $= 2 bc_o \left(\frac{t_o}{c_o}\right) \left(\frac{x}{c_o}\right)^2 \left(1 - \frac{x}{c_o}\right) \left(2 - \frac{x}{c_o}\right)$ |
| Wing volume | $= \frac{7}{30} bc_o^2 \left(\frac{t_o}{c_o}\right)$ |

## 2.2 Description of tests

Six component balance measurements were made at speeds ranging from 80 ft/sec. to 300 ft/sec., giving Reynolds' Numbers (based on aerodynamic mean chord $\bar{\bar{c}}$) of $2.3 \times 10^6$ to $8.6 \times 10^6$. Due to rig loads, the highest speed could cover only a limited incidence range, while the lowest speed was necessary to reach the maximum lift coefficient. All force and moment coefficients are quoted relative to wind axes, a diagram of the axes system being shown in Fig.3.

To aid in the study of the regions of separated flow, two visualisation techniques were used in conjunction with each other. Firstly, the oil flow method, using a mixture of titanium oxide in diesel oil with a small quantity of oleic acid, at a tunnel speed of 150 ft/sec. To assist in interpretation of photographs, a graduated rectangular frame was suspended round the model when photographs were taken (Figs. 21, 22). The divisions are tenths of the root chord and tenths of the semi-span in chordwise and spanwise directions respectively. Secondly, the smoke technique described in Ref.6 was used at a tunnel speed of 50 ft/sec. Photographs were taken using an exposure of 1/10 sec. at f4.5 with fast plates and normal development.

## 3 Flow observations

The flow separates all along the sharp leading edges and vorticity is shed, which rolls up to form coiled vortex sheets with a "core" of high vorticity above and inside the leading edges. These vortex sheets become a dominating feature of the flow at high incidences as can be seen in the photographs of Figs.18, 19. Throughout the whole incidence range tested ($0^\circ$ to $45^\circ$) the separated flow pattern was perfectly steady, symmetrical and repeatable.

Over the whole range of practical flight incidences the flow is of one type, with rolled-up vortex sheets which grow in size and move inboard with increasing incidence. This type of flow is maintained to above $C_{L_{max}}$, the vortex sheets still growing in size with incidence, but their cores become less defined and no longer move inwards towards each other. At the same time, a separation bubble starts to form near

the trailing edge on the wing surface outboard of each vortex sheet; this can be seen in the photograph of the oil flow pattern at $\alpha = 31.6^{\circ}$ in Fig.21.

Using the smoke technique, the position of the vortex sheet cores was measured at a number of chordwise stations over the incidence range $10^{\circ}$-$40^{\circ}$; the results are plotted in Figs. 4 and 5. In side elevation, the core path appears to be straight from the leading-edge apex back as far as the trailing edge region, after which it curves downstream. Assuming a straight path from the apex, it is possible to calculate the angle between the core path and the wing chordal plane as $\theta = \tan^{-1} z/x$ . These values are plotted in Fig.4 and show that $\theta/\alpha$ is very nearly constant and equals approximately 0.3. There is a tendency for slightly higher values to occur over the central region of the wing, which is probably due to a displacement effect of the wing thickness. Plotted in Fig.4 as broken lines are the theoretical estimates of Mangler and Smith[7] for a flat plate wing at incidences of $15^{\circ}$ and $30^{\circ}$, which agree closely with the experimental results. In plan view (Fig.5), the path of the core is found to be a curve similar in shape to the leading edge, lying about 0.8 of the local span out from the wing centre line at an incidence of $20^{\circ}$. Initially, the core moves inwards quite rapidly with increasing incidence, but this movement becomes less rapid as higher incidences are reached. At all incidences the cores were further outboard than on comparable delta wings, as can be seen by comparison with Fig.6 of Ref.1.

At speeds greater than 150 ft/sec. and incidences between $20^{\circ}$ and $30^{\circ}$, the decrease in temperature due to expansion in the low-pressure cores of the vortex sheets was sufficient to cause water vapour condensation - this revealing the path of the cores. Photographs of this phenomenon at a wing incidence of $24^{\circ}$ are given in Fig.20. Incidence-telescope measurements confirmed that the angle between the core path and the wing chordal plane is 0.3 of the incidence (as found with the smoke technique), indicating that Reynolds' Number has no appreciable effect on the geometry of the separated flow. As the incidence was increased above $25^{\circ}$, the length of visible core decreased, until at $30^{\circ}$ incidence only about a 1/4-root-chord length could be seen. A similar effect was noticed when the model was yawed; at $25^{\circ}$ incidence and $3^{\circ}$ yaw, the core on the trailing-wing side was visible for about three-root-chord lengths downstream of the trailing edge, while on the leading-wing the visible length had shortened to about one-half of a root-chord. The condensation trail appeared to "bell-out" before disappearing - as though the core was becoming more diffuse. This suggests that the geometry of the rolling-up process varies, only certain conditions giving a concentrated core of very low pressure. This phenomenon also confirmed that the position of the vortex sheets was perfectly steady.

The development of the vortex sheets can be seen in the photographs of Figs.18, 19, and their effect on the wing surface at various incidences is shown by the oil flow patterns of Figs. 21, 22. It is basically the same as that on a delta, as described by Weber[1] and Maskell[8], except that the vortex sheet cores follow a curved path similar in shape to the leading edge. A large photograph of the surface oil flow pattern at an incidence of $21.2^{\circ}$ is reproduced in Fig.22 and the various features identified. Of the air which flows close over the top of the vortex sheets, part is drawn down towards the wing and flows downstream along the surface - giving the region (A) in Fig.22; air which flows closer to the vortex sheets is drawn into them. The dividing line on the upper surface of the wing between the two flows is an "attachment line" as defined by Maskell[8]. Outside this line,* the surface streamlines are curved - region (B) in Fig.22, the position of the maximum spanwise velocity showing as a point of inflection of the streamlines. (One normally identifies this inflection with the peak suction, but this has not been checked here.) Measurements show that a normal from

---

* These considerations do not, of course, apply to the immediate neighbourhood of the trailing edge which itself is another separation line.

the wing surface at this point of inflection intersects the core of the vortex sheet, the effect of wing thickness probably keeping the core further away from the wing centre line as compared with a flat plate wing. It also means that the peak suction line is always inboard of the vortex sheet cores on a wing with thickness. A secondary separation occurs outboard of the peak suction line - region (C) in Fig.22, leaving a region in which the total head is usually found to be low, between there and the leading edge. No vorticity was apparent in this region in the smoke tests, but a weak inflow towards the secondary separation line was evident in the surface oil flow suggesting a slow rotation of the low-energy air there in a direction opposite to that of the leading edge vortex sheet, consistent with the theory of Maskell[8]. The movement with incidence of the point of inflection line, attachment line and the secondary separation line is plotted in Figs.6 and 7.

Above the upper surface of the wing, outboard of the attachment lines, there is a strong outflow caused by each leading-edge vortex sheet, while below the lower surface the flow is approximately chordwise in direction. This causes a vorticity distribution in the free sheet leaving the trailing edge which is opposite in sign to that of the leading edge vortex sheet. The vortex sheet from the trailing edge then deforms in an unusual manner, and rolls up to form a small coil of opposite sign adjacent to the coil of normal sign from each leading-edge sheet. As the sheets move downstream, the pair at each tip rotate about each other in the direction of the leading-edge vortex sheet. This process can be seen in the photographs of Figs.18, 19.

When the wing was yawed, the cross-section shape of the vortex sheet on the leading wing became oval with a poorly defined core, while the vortex sheet on the trailing wing became more circular in section with a well defined core. In addition, the regions of the wing upper surface affected by the vortex sheets changed, the suctions induced by them acting over a greater area on the leading wing. As this suction acts on a sideways sloping surface, a positive yaw results in a positive rolling moment and a negative side force.

## 4 Overall forces and moments

### 4.1 Correction of balance measurements

Because of the uncertainty of what corrections should be applied to allow for tunnel interference effects on wings of low aspect ratio with separated flow, two similar models - of wing areas 16 $ft^2$ and 4 $ft^2$ - were tested at the same Reynolds' Number over an incidence range of $0^\circ$-$40^\circ$, with the aim of deducing an empirical correction method from the results.

The corrections for interference effects were applied in the following order:-

(i) A correction to incidence to allow for boundary constraint and induced curvature of flow (lift effects).

(ii) Arising from (i), the measured coefficients were resolved relative to the corrected wind direction.

(iii) All coefficients were corrected for the effects of solid blockage and wake blockage, the wake blockage correction being adjusted until agreement was reached between the results for both models.

To correct for the effect of boundary constraint, the measured incidence was increased by an amount, $\Delta\alpha$ , calculated from

$$\Delta\alpha = \lambda_\alpha \quad SC_L$$

the value of $\lambda_\alpha$ being found from Ref. 9, with an addition of $0.00585\bar{\bar{c}}$ to allow for induced curvature of flow as suggested by Batchelor in Ref.10. For a delta wing of aspect ratio 1.0, the value obtained by this method agrees with that obtained using the expression for $\lambda_\alpha$ given by Acum in Ref.11:-

$$\lambda_\alpha = \lambda_1 + \lambda_2 c_o + \lambda_3 [\tan \Lambda_1 - \tan \Lambda_2]$$

but for the Gothic shape it is difficult to estimate realistic values of the 1/4-chord and 3/4 chord angles of sweep, $\Lambda_1$ and $\Lambda_2$.

As the effect of boundary constraint is to increase the effective incidence by $\Delta\alpha$, the lift and drag coefficients $C_L'$ and $C_D'$ measured perpendicular and parallel to the direction of the undisturbed flow (i.e. the tunnel axis), must be corrected to give components $C_L''$ and $C_D''$ relative to the effective wind direction.

Resolution of the measured coefficients relative to this effective wind direction gives:-

$$C_L'' = C_L' \cos\Delta\alpha - C_D' \sin\Delta\alpha \simeq C_L' - C_D' . \Delta\alpha$$

$$C_D'' = C_D' \cos\Delta\alpha + C_L' \sin\Delta\alpha \simeq C_D' + C_L' . \Delta\alpha$$

The term $C_D'.\Delta\alpha$ cannot be neglected, as is often the case, as at high incidences the lift and drag coefficients are of the same order of magnitude.

The lift curves for the two models, corrected up to this stage, are plotted in Fig.8; also shown is the uncorrected lift curve for the larger model. It appears that the correction for lift effect is satisfactory, as the results agree up to a $C_L$ of 1.0, but after there the curves diverge, the ultimate difference in $C_{L_{max}}$ being about 0.2. It has been assumed that this divergence is solely due to the effect of wake blockage and this view is supported by the fact that $C_D$ rises more steeply above a $C_L$ of about 1.0.

To correct for blockage, the coefficients already corrected for lift effects were multiplied by $(1 - 2\varepsilon)$, $\varepsilon$ being the sum of the solid blockage (usually small) and wake blockage factors $\varepsilon_1$ and $\varepsilon_2$ respectively, and is defined by:-

$$V_T = V_o (1 + \varepsilon)$$

where $V_T$ = speed in tunnel with model present

$V_o$ = speed in tunnel without model.

The solid and wake blockage corrections were calculated from the following expressions, given in Ref.12.

Solid blockage factor $\varepsilon_1 = G\left(1 + 1.2\,\frac{t}{c}\right)\frac{w}{C^{3/2}}$

Wake blockage factor $\varepsilon_2 = \frac{C_{D_{wake}} S}{4C}$

where $w$ = model volume

$C$ = working section cross-section area

$G$ = factor depending on tunnel proportions

Work done by Maskell[13] on flow with separations, suggests that the wake drag coefficient is given by an expression of the form

$$C_{D_{wake}} = \left(C_{D_o} + C_{D_{rig}}\right) + F\left(C_D - C_{D_o} - \frac{kC_L^2}{\pi A}\right)$$

where $F$ = a factor depending on the nature of the wake

$k$ = a drag-due-to-lift factor

For the results in this report, $k$ has been calculated from the mean slope of the $0.2 < C_L < 1.0$ region of the $C_D/C_L^2$ curve (uncorrected for blockage) for each model, and a value of $F$ found which gave agreement between the two model tests. By this method, it is found that the $C_{L_{max}}$ values agree if a value of 6 is used for the factor $F$. The fully corrected values are shown as plotted points in Fig.8.

Comparison of the corrected and uncorrected results in Fig.8, shows that even for a normal size model the correction is comparatively large. (The model wing area of 16 $ft^2$ is approximately $1/7$th of the cross-section area of the working section). Thus care must be taken when the results in this report are compared with other tests where an adequate correction may not have been applied.

## 4.2 Scale effect

Lift, drag and pitching moment coefficients measured at various Reynolds' Numbers between $2.3 \times 10^6$ and $8.6 \times 10^6$ are presented in Table I. Apart from small differences in the drag coefficient at low incidences, the results are unaffected by Reynolds' Number. This is presumably because its major effect of modifying separation conditions is absent, the flow separations being fixed at the sharp edges of the wing.

## 4.3 Discussion of results

Where possible, characteristics of the Gothic wing tested are compared with results for similar wings given by Weber in Ref.1. However, this report only contains results on sharp-edged flat plate wings and finite thickness wings with round leading edges, so the results are not strictly comparable. Also, there are probably some differences in corrections for tunnel interference effects.

The lift and pitching moment coefficients are plotted in Fig.9, and it can be seen that the Gothic wing curves lie between those of a delta, and a taper-ratio 0.5 cropped-delta of the same aspect ratio. The maximum lift coefficient of the Gothic wing is, however, higher than both, showing an increase of 0.3 over the delta. The non-linear lift only builds up

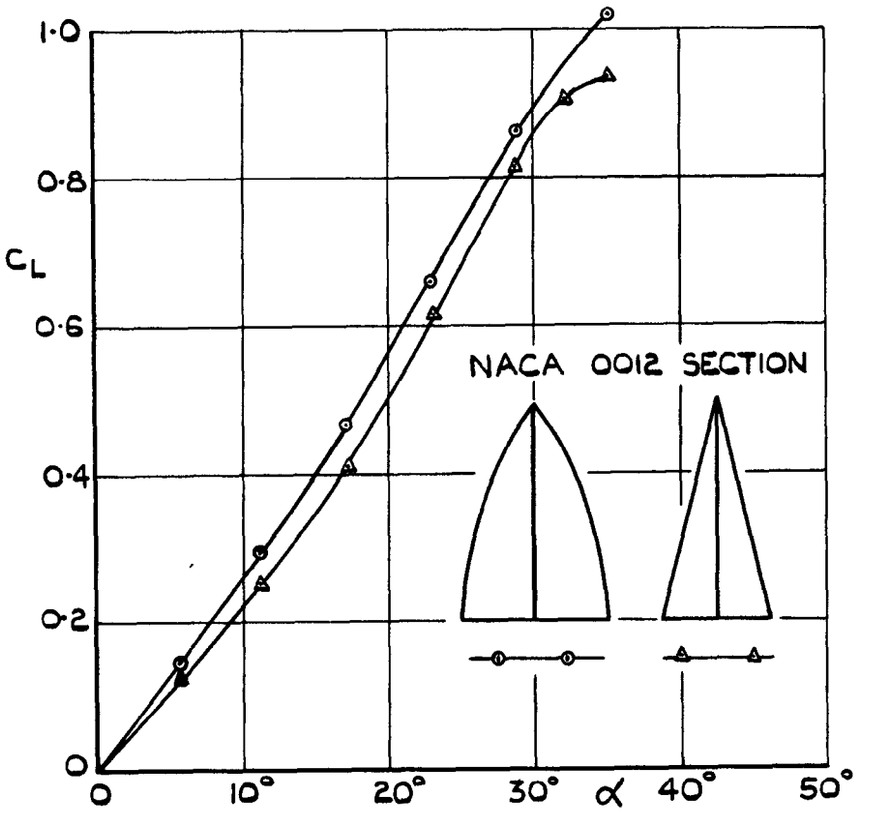


(a) ROUND L.E. REF. 4.

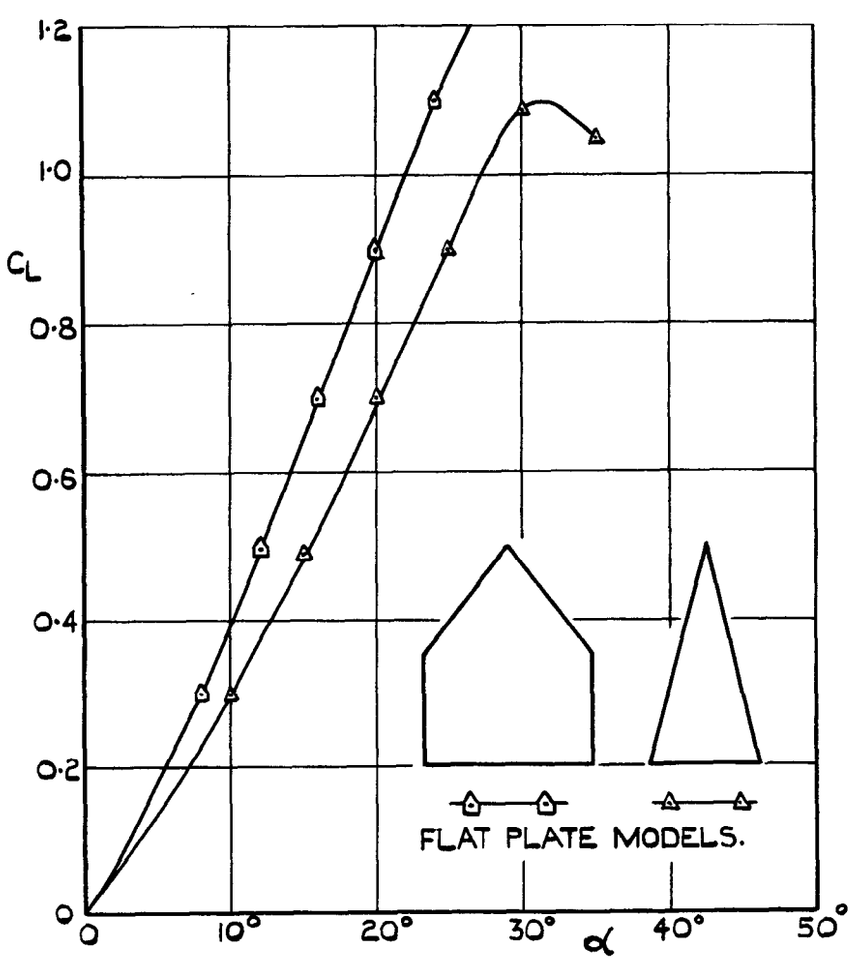


(b) SHARP L.E. REF. 1. FIG. 13.

FIG. 1 (a & b) LIFT CHARACTERISTICS OF ASPECT RATIO 1·0 WINGS WITH UNSWEPT TRAILING EDGES.

(iii) Using aspect ratio as the criterion, the Gothic wing had better lift and drag characteristics than a delta wing. Putting this another way, the lift and drag characteristics of a delta wing could be obtained by a Gothic wing of lower aspect ratio; results suggest that the ratio span/root chord is a possible correlating factor.

(iv) Tunnel interference corrections were large, even though the model was of average size. Thus existing data, to which adequate corrections may not have been applied, becomes suspect.

Future work includes tests on a delta wing of aspect ratio 1.0 with a 12% biconvex root section, and diamond-shaped cross-sections; also two flat plate models of the Gothic and delta wing planforms. It is hoped that from these tests, the separate effects of planform shape and thickness distribution will be determined.

---

## LIST OF SYMBOLS

| | |
|---|---|
| $x, y, z$ | rectangular body co-ordinates, x chordwise from apex, y spanwise |
| $c_o$ | wing root chord |
| $s(x)$ | local semi-span |
| $b$ | wing span |
| $t_o$ | maximum thickness of centre line aerofoil section |
| $\alpha$ | angle of incidence |
| $\psi$ | angle of yaw, positive to starboard |
| $\beta$ | angle of sideslip $(= -\psi)$ |
| $C_L$ | overall lift coefficient |
| $C_D$ | overall drag coefficient |
| $C_M$ | overall pitching moment coefficient, referred to aerodynamic mean chord, taken about mean quarter chord |
| $C_{\mathcal{L}}$ | rolling moment coefficient, positive starboard wing down |
| $C_N$ | yawing moment coefficient about quarter chord point, positive to starboard |
| $C_y$ | side force coefficient, positive to starboard |
| $C_T$ | tangential force coefficient |
| $K$ | $\dfrac{C_D - C_{D_o}}{C_L^2 / \pi A}$, drag factor |
| $K'$ | mean slope of near-linear part of corrected $C_D/C_L^2$ curve |
| $k$ | mean slope of near-linear part of uncorrected $C_D/C_L^2$ curve |

## LIST OF SYMBOLS (contd.)

| | |
|---|---|
| $\ell_v$ | $\frac{dC_\ell}{d\beta}$ per radian |
| $n_v$ | $\frac{dC_N}{d\beta}$ per radian |
| $y_v$ | $\frac{dC_Y}{d\beta}$ per radian |
| $C'_L$, $C'_D$ | measured lift and drag coefficients relative to tunnel axis, uncorrected for blockage |
| $C''_L$, $C''_D$ | lift and drag coefficients resolved perpendicular and parallel to effective wind direction, uncorrected for blockage |
| $\lambda_1$, $\lambda_2$, $\lambda_3$ | factors depending on tunnel proportions |
| $C_{L_{lin}}$ | theoretical linear lift coefficient |
| $C_{L_{exp}}$ | experimental value of lift coefficient. |

---

## REFERENCES


| No. | Author | Title, etc. |
|---|---|---|
| 1 | Weber, J. | Some effects of flow separation on slender delta wings. R.A.E. Tech. Note Aero.2425. A.R.C. 18073. Nov.1955. |
| 2 | Peckham, D. H. | The geometry of wing surfaces generated by straight lines and with a high rate of thickness taper at the root. C.P. 383. May 1957. |
| 3 | Voepel, H. | Tests on wings of small aspect ratio. Ed. F.N. Kirk R.A.E. Library Trans. 276. Oct. 1948. |
| 4 | Gdaliahu, M. | A summary of the results of some German model tests on wings of small aspect ratio. A.R.C. 9638. March 1946. |
| 5 | Newby, K.W. | The effects of taper on the supervelocities on three-dimensional wings at zero incidence. R. & M. 3032. June 1955. |
| 6 | Maltby, R. L. and Peckham, D. H. | Low speed flow studies of the vortex patterns above inclined slender bodies using a new smoke technique. A.R.C. 19,541. Nov. 1956. Addendum, March 1957. |
| 7 | Mangler, K. W. and Smith, J. H. B. | A theory of separation from the curved leading edge of a slender wing. (To be published) |

REFERENCES (contd.)


| No. | Author | Title, etc. |
|---|---|---|
| 8 | Maskell, E. C. | Flow separation in three dimensions. A.R.C. 18,063. Nov. 1955. |
| 9 | Glauert, H. | Wind tunnel interference on wings bodies and airscrews. R. & M. 1566. 1933. |
| 10 | Batchelor, G. K. | The interference of wings bodies and airscrews in a closed tunnel of octagonal section. Australia C.S.I.R. Rept A.19. A.R.C. 7491. Oct. 1943. |
| 11 | Acum, W. E. A. | Corrections for symmetrical swept and tapered wings in rectangular wind tunnels. A.R.C. 14159. 1951. |
| 12 | Thompson, J. S. | Present methods of applying blockage corrections in a closed rectangular high speed tunnel. A.R.C. 11,385. Jan. 1948. |
| 13 | Maskell, E. C. | A theory of wind tunnel blockage effects on stalled flows. (To be published as R.A.E. Report) |

TABLE I

Coefficients of overall lift, drag and pitching moment at zero yaw

| V = 102 ft/sec. R = 2.9 × $10^6$ | | | |
|---|---|---|---|
| $\alpha$ | $C_L$ | $C_D$ | $C_M$ |
| 0.10 | 0.002 | 0.0056 | -0.0007 |
| 2.16 | 0.049 | 0.0091 | -0.0019 |
| 4.24 | 0.113 | 0.0149 | -0.0079 |
| 6.38 | 0.183 | 0.0246 | -0.0151 |
| 8.48 | 0.260 | 0.0410 | -0.0223 |
| 10.59 | 0.345 | 0.0619 | -0.0310 |
| 12.71 | 0.435 | 0.0916 | -0.0410 |
| 14.83 | 0.532 | 0.1295 | -0.0514 |
| 17.01 | 0.633 | 0.1761 | -0.0628 |
| 19.14 | 0.732 | 0.2314 | -0.0745 |
| 21.28 | 0.841 | 0.2966 | -0.0872 |
| 23.47 | 0.953 | 0.3753 | -0.1001 |
| 25.56 | 1.060 | 0.4619 | -0.1121 |
| 27.66 | 1.142 | 0.5437 | -0.1190 |
| 29.76 | 1.221 | 0.6339 | -0.1296 |
| 31.86 | 1.301 | 0.7450 | -0.1438 |
| 33.83 | 1.353 | 0.8428 | -0.1540 |
| 35.88 | 1.390 | 0.9296 | -0.1601 |

| V = 81 ft/sec. R = 2.3 × $10^6$ | | | |
|---|---|---|---|
| $\alpha$ | $C_L$ | $C_D$ | $C_M$ |
| 37.90 | 1.408 | 1.012 | -0.1648 |
| 39.92 | 1.387 | 1.083 | -0.1723 |
| 41.86 | 1.372 | 1.153 | -0.1809 |
| 43.89 | 1.319 | 1.184 | -0.1952 |

| V = 152 ft/sec. R = 4.3 × $10^6$ | | | |
|---|---|---|---|
| $\alpha$ | $C_L$ | $C_D$ | $C_M$ |
| 0.10 | 0.003 | 0.0057 | -0.0004 |
| 2.22 | 0.053 | 0.0089 | -0.0022 |
| 4.30 | 0.117 | 0.0120 | -0.0082 |
| 6.39 | 0.187 | 0.0244 | -0.0115 |
| 8.54 | 0.266 | 0.0405 | -0.0226 |
| 10.65 | 0.349 | 0.0630 | -0.0307 |
| 12.86 | 0.441 | 0.0933 | -0.0405 |
| 14.99 | 0.541 | 0.1330 | -0.0511 |
| 17.16 | 0.636 | 0.1792 | -0.0625 |
| 19.30 | 0.745 | 0.2376 | -0.0752 |
| 21.43 | 0.850 | 0.3044 | -0.0878 |
| 23.61 | 0.963 | 0.3849 | -0.1009 |
| 25.84 | 1.073 | 0.4748 | -0.1168 |

| V = 202 ft/sec. R = 5.7 × $10^6$ | | | |
|---|---|---|---|
| $\alpha$ | $C_L$ | $C_D$ | $C_M$ |
| 0.15 | 0.003 | 0.0062 | 0.0005 |
| 2.22 | 0.055 | 0.0085 | -0.0029 |
| 4.35 | 0.119 | 0.0141 | -0.0087 |
| 6.44 | 0.190 | 0.0242 | -0.0153 |
| 8.60 | 0.270 | 0.0407 | -0.0233 |
| 10.75 | 0.355 | 0.0634 | -0.0318 |
| 12.92 | 0.449 | 0.0950 | -0.0419 |
| 15.15 | 0.548 | 0.1355 | -0.0530 |
| 17.38 | 0.652 | 0.1847 | -0.0651 |
| 19.57 | 0.759 | 0.2444 | -0.0778 |
| 21.82 | 0.872 | 0.3169 | - |

| V = 303 ft/sec. R = 8.6 × $10^6$ | | | |
|---|---|---|---|
| $\alpha$ | $C_L$ | $C_D$ | $C_M$ |
| 0.15 | 0.004 | 0.0076 | 0.0002 |
| 2.22 | 0.054 | 0.0096 | -0.0033 |
| 4.36 | 0.123 | 0.0153 | -0.0096 |
| 6.45 | 0.193 | 0.0257 | -0.0162 |
| 8.65 | 0.276 | 0.0433 | -0.0244 |
| 10.87 | 0.367 | 0.0682 | -0.0340 |

TABLE II

Coefficients of overall side force, rolling moment and yawing moment

| $\alpha$ = 0° V = 202 ft/sec. R = 5.7 × $10^6$ | | | | | | |
|---|---|---|---|---|---|---|
| $\beta$ | $C_L$ | $C_D$ | $C_M$ | $C_y$ | $C_\ell$ | $C_N$ |
| 5.0 | -0.001 | 0.0060 | 0.0008 | -0.0003 | 0 | 0.0003 |
| 2.5 | 0 | 0.0057 | 0.0007 | -0.0001 | 0 | 0.0005 |
| 0 | 0 | 0.0056 | 0.0004 | -0.0001 | 0 | 0.0010 |
| - 2.5 | 0 | 0.0057 | 0.0006 | -0.0001 | 0 | 0.0016 |
| - 5.0 | -0.001 | 0.0059 | 0.0006 | 0 | 0 | 0.0021 |
| -10.0 | -0.001 | 0.0062 | 0.0008 | 0.0003 | 0 | 0.0030 |
| -15.0 | -0.002 | 0.0063 | 0.0009 | 0.0008 | 0 | 0.0040 |

| $\alpha$ = 4.34° V = 202 ft/sec. R = 5.7 × $10^6$ | | | | | | |
|---|---|---|---|---|---|---|
| $\beta$ | $C_L$ | $C_D$ | $C_M$ | $C_y$ | $C_\ell$ | $C_N$ |
| 5.0 | 0.116 | 0.0138 | -0.0087 | 0.0004 | -0.0061 | 0.0004 |
| 2.5 | 0.116 | 0.0139 | -0.0090 | 0.0001 | -0.0034 | 0.0006 |
| 0 | 0.116 | 0.0138 | -0.0090 | -0.0003 | -0.0002 | 0.0010 |
| - 2.5 | 0.116 | 0.0138 | -0.0090 | -0.0005 | 0.0030 | 0.0011 |
| - 5.0 | 0.115 | 0.0138 | -0.0086 | -0.0009 | 0.0060 | 0.0014 |
| -10.0 | 0.114 | 0.0137 | -0.0074 | -0.0024 | 0.0117 | 0.0020 |
| -15.0 | 0.110 | 0.0135 | -0.0057 | -0.0025 | 0.0165 | 0.0025 |

| $\alpha$ = 8.53° V = 202 ft/sec. R = 5.7 × $10^6$ | | | | | | |
|---|---|---|---|---|---|---|
| $\beta$ | $C_L$ | $C_D$ | $C_M$ | $C_y$ | $C_\ell$ | $C_N$ |
| 5.0 | 0.269 | 0.0407 | -0.0231 | 0.0040 | -0.0135 | 0.0019 |
| 2.5 | 0.269 | 0.0409 | -0.0238 | 0.0024 | -0.0068 | 0.0014 |
| 0 | 0.269 | 0.0409 | -0.0240 | 0.0005 | 0.0001 | 0.0008 |
| - 2.5 | 0.269 | 0.0409 | -0.0238 | -0.0012 | 0.0070 | 0.0003 |
| - 5.0 | 0.268 | 0.0409 | -0.0232 | -0.0025 | 0.0136 | -0.0003 |
| -10.0 | 0.267 | 0.0405 | -0.0209 | -0.0061 | 0.0263 | -0.0012 |
| -15.0 | 0.260 | 0.0382 | -0.0165 | -0.0102 | 0.0364 | -0.0019 |

| $\alpha$ = 12.71° V = 152 ft/sec. R = 4.3 × $10^6$ | | | | | | |
|---|---|---|---|---|---|---|
| $\beta$ | $C_L$ | $C_D$ | $C_M$ | $C_y$ | $C_\ell$ | $C_N$ |
| 5.0 | 0.443 | 0.0924 | -0.0400 | 0.0103 | -0.0211 | 0.0044 |
| 2.5 | 0.443 | 0.0927 | -0.0408 | 0.0055 | -0.0106 | 0.0027 |
| 0 | 0.444 | 0.0927 | -0.0410 | 0.0008 | 0.0004 | 0.0005 |
| - 2.5 | 0.444 | 0.0926 | -0.0410 | -0.0040 | 0.0111 | -0.0015 |
| - 5.0 | 0.443 | 0.0924 | -0.0398 | -0.0086 | 0.0215 | -0.0033 |
| -10.0 | 0.435 | 0.0922 | -0.0344 | -0.0173 | 0.0396 | -0.0071 |
| -15.0 | 0.421 | 0.0858 | -0.0256 | -0.0247 | 0.0528 | -0.0090 |

TABLE II (Contd.)

| $\alpha$ = 17.01° | V = 102 ft/sec. | | R = 2.9 × $10^6$ | | | |
|---|---|---|---|---|---|---|
| $\beta$ | $C_L$ | $C_D$ | $C_M$ | $C_y$ | $C_\ell$ | $C_N$ |
| 5.0 | 0.622 | 0.1744 | -0.0579 | 0.0191 | -0.0311 | 0.0074 |
| 2.5 | 0.622 | 0.1762 | -0.0602 | 0.0098 | -0.0168 | 0.0041 |
| 0 | 0.630 | 0.1768 | -0.0628 | 0.0005 | -0.0018 | 0.0002 |
| - 2.5 | 0.629 | 0.1763 | -0.0638 | -0.0088 | 0.0129 | -0.0037 |
| - 5.0 | 0.621 | 0.1736 | -0.0577 | -0.0181 | 0.0282 | -0.0070 |
| -10.0 | 0.596 | 0.1666 | -0.0489 | -0.0335 | 0.0487 | -0.0131 |
| -15.0 | 0.572 | 0.1571 | -0.0374 | -0.0479 | 0.0675 | -0.0177 |

| $\alpha$ = 21.28° | V = 102 ft/sec. | | R = 2.9 × $10^6$ | | | |
|---|---|---|---|---|---|---|
| $\beta$ | $C_L$ | $C_D$ | $C_M$ | $C_y$ | $C_\ell$ | $C_N$ |
| 5.0 | 0.820 | 0.2913 | -0.0811 | 0.0294 | -0.0334 | 0.0122 |
| 2.5 | 0.832 | 0.2958 | -0.0844 | 0.0154 | -0.0170 | 0.0063 |
| 0 | 0.837 | 0.2979 | -0.0868 | 0.0016 | 0.0005 | 0.0001 |
| - 2.5 | 0.827 | 0.2937 | -0.0826 | -0.0139 | 0.0181 | -0.0058 |
| - 5.0 | 0.819 | 0.2906 | -0.0803 | -0.0279 | 0.0343 | -0.0116 |
| -10.0 | 0.779 | 0.2771 | -0.0700 | -0.0516 | 0.0584 | -0.0201 |
| -15.0 | 0.725 | 0.2544 | -0.0520 | -0.0733 | 0.0731 | -0.0251 |

| $\alpha$ = 25.57° | V = 102 ft/sec. | | R = 2.9 × $10^6$ | | | |
|---|---|---|---|---|---|---|
| $\beta$ | $C_L$ | $C_D$ | $C_M$ | $C_y$ | $C_\ell$ | $C_N$ |
| 5.0 | 1.028 | 0.4504 | -0.1091 | 0.0419 | -0.0392 | 0.0164 |
| 2.5 | 1.034 | 0.4528 | -0.1076 | 0.0207 | -0.0182 | 0.0081 |
| 0 | 1.056 | 0.4621 | -0.1121 | 0.0005 | 0.0012 | -0.0004 |
| -. 2.5 | 1.036 | 0.4532 | -0.1090 | -0.0201 | 0.0203 | -0.0083 |
| - 5.0 | 1.023 | 0.4473 | -0.1081 | -0.0413 | 0.0408 | -0.0165 |
| -10.0 | 0.971 | 0.4234 | -0.0960 | -0.0776 | 0.0694 | -0.0275 |
| -15.0 | 0.859 | 0.3745 | -0.0719 | -0.0988 | 0.0726 | -0.0279 |

| $\alpha$ = 29.76° | V = 102 ft/sec. | | R = 2.9 × $10^6$ | | | |
|---|---|---|---|---|---|---|
| $\beta$ | $C_L$ | $C_D$ | $C_M$ | $C_y$ | $C_\ell$ | $C_N$ |
| 5.0 | 1.204 | 0.6327 | -0.1344 | 0.0534 | -0.0416 | 0.0194 |
| 2.5 | 1.222 | 0.6428 | -0.1364 | 0.0257 | -0.0183 | 0.0089 |
| 0 | 1.213 | 0.6365 | -0.1341 | -0.0016 | 0.0014 | -0.0007 |
| - 2.5 | 1.221 | 0.6409 | -0.1357 | -0.0277 | 0.0217 | -0.0104 |
| - 5.0 | 1.202 | 0.6309 | -0.1346 | -0.0549 | 0.0442 | -0.0204 |
| -10.0 | 1.136 | 0.5938 | -0.1204 | -0.1037 | 0.0765 | -0.0355 |
| -15.0 | 0.963 | 0.5120 | -0.1046 | -0.1206 | 0.0727 | -0.0263 |

TABLE II (Contd.)

| $\alpha = 33.83^\circ$ | V = 102 ft/sec. | | R = $2.9 \times 10^6$ | | | |
|---|---|---|---|---|---|---|
| $\beta$ | $C_L$ | $C_D$ | $C_M$ | $C_y$ | $C_\ell$ | $C_N$ |
| 5.0 | 1.336 | 0.8312 | -0.1480 | 0.0631 | -0.0396 | 0.0194 |
| 2.5 | 1.344 | 0.8357 | -0.1455 | 0.0311 | -0.0210 | 0.0106 |
| 0 | 1.344 | 0.8353 | -0.1432 | -0.0034 | 0.0020 | -0.0011 |
| -2.5 | 1.343 | 0.8336 | -0.1445 | -0.0366 | 0.0242 | -0.0122 |
| -5.0 | 1.334 | 0.8298 | -0.1512 | -0.0677 | 0.0416 | -0.0195 |

| $\alpha = 37.90^\circ$ | V = 81 ft/sec. | | R = $2.3 \times 10^6$ | | | |
|---|---|---|---|---|---|---|
| $\beta$ | $C_L$ | $C_D$ | $C_M$ | $C_y$ | $C_\ell$ | $C_N$ |
| 5.0 | 1.375 | 0.9863 | -0.1528 | 0.0715 | -0.0366 | 0.0170 |
| 2.5 | 1.394 | 1.0032 | -0.1616 | 0.0346 | -0.0194 | 0.0094 |
| 0 | 1.401 | 1.0087 | -0.1592 | -0.0053 | 0.0017 | -0.0013 |
| -2.5 | 1.403 | 1.0100 | -0.1636 | -0.0429 | 0.0237 | -0.0099 |
| -5.0 | 1.375 | 0.9884 | -0.1641 | -0.0806 | 0.0412 | -0.0176 |



W.T.2078.C.P.505.K3 - Printed in England

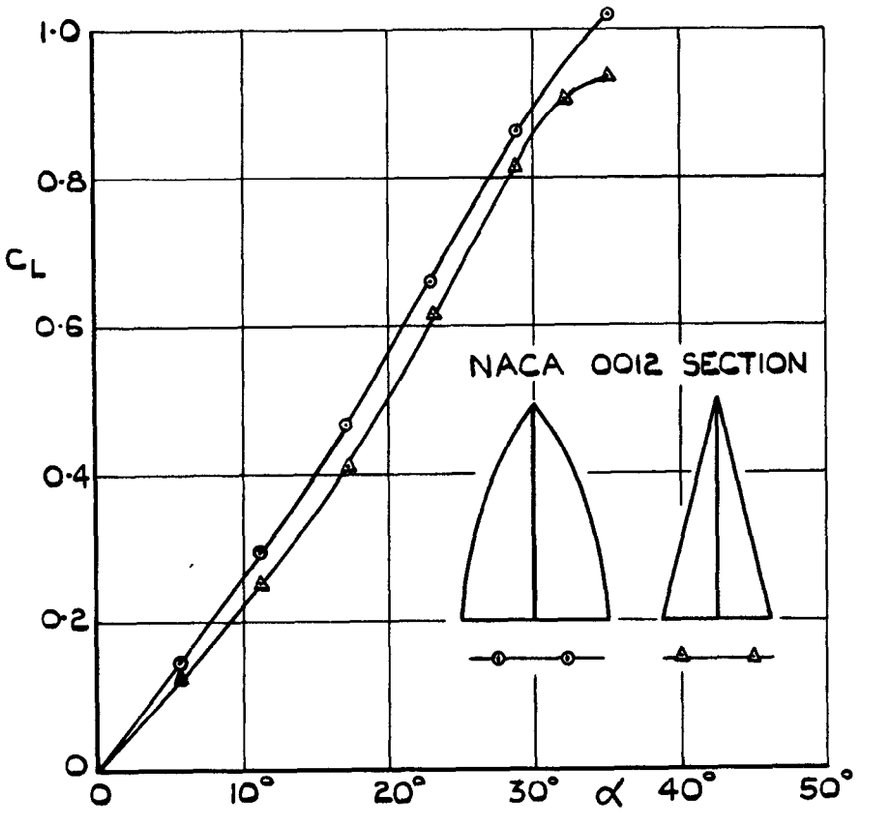


(a) ROUND L.E. REF. 4.

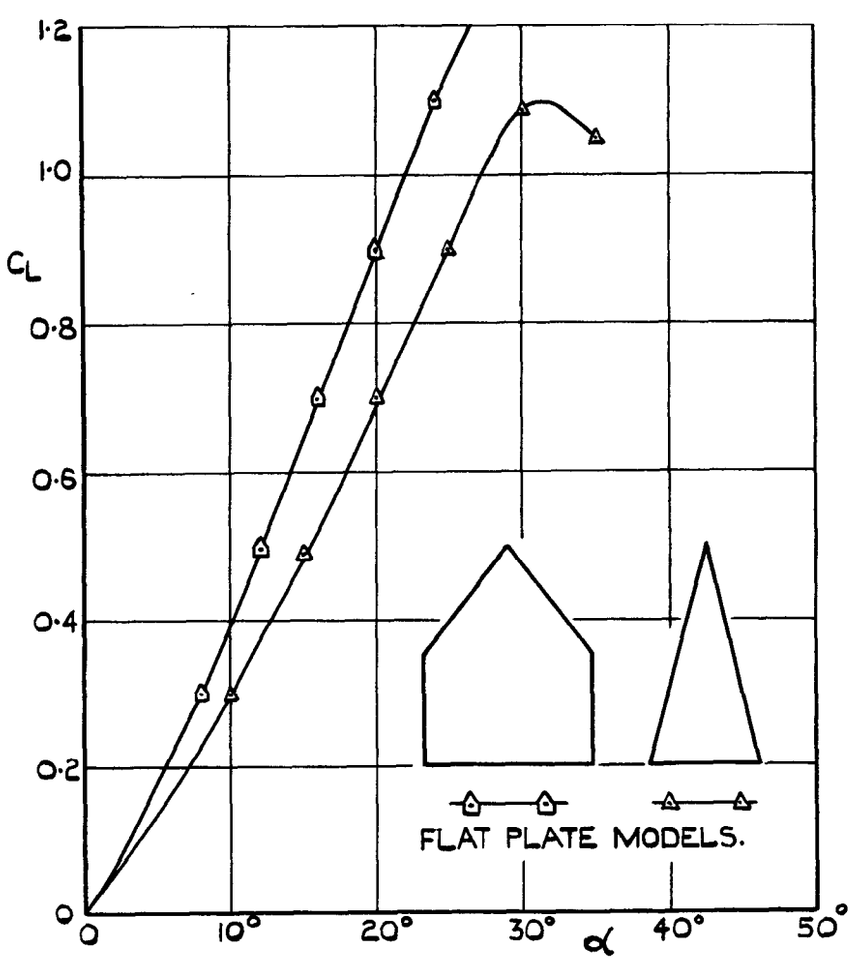


(b) SHARP L.E. REF. 1. FIG. 13.

FIG. 1 (a & b) LIFT CHARACTERISTICS OF ASPECT RATIO 1·0 WINGS WITH UNSWEPT TRAILING EDGES.

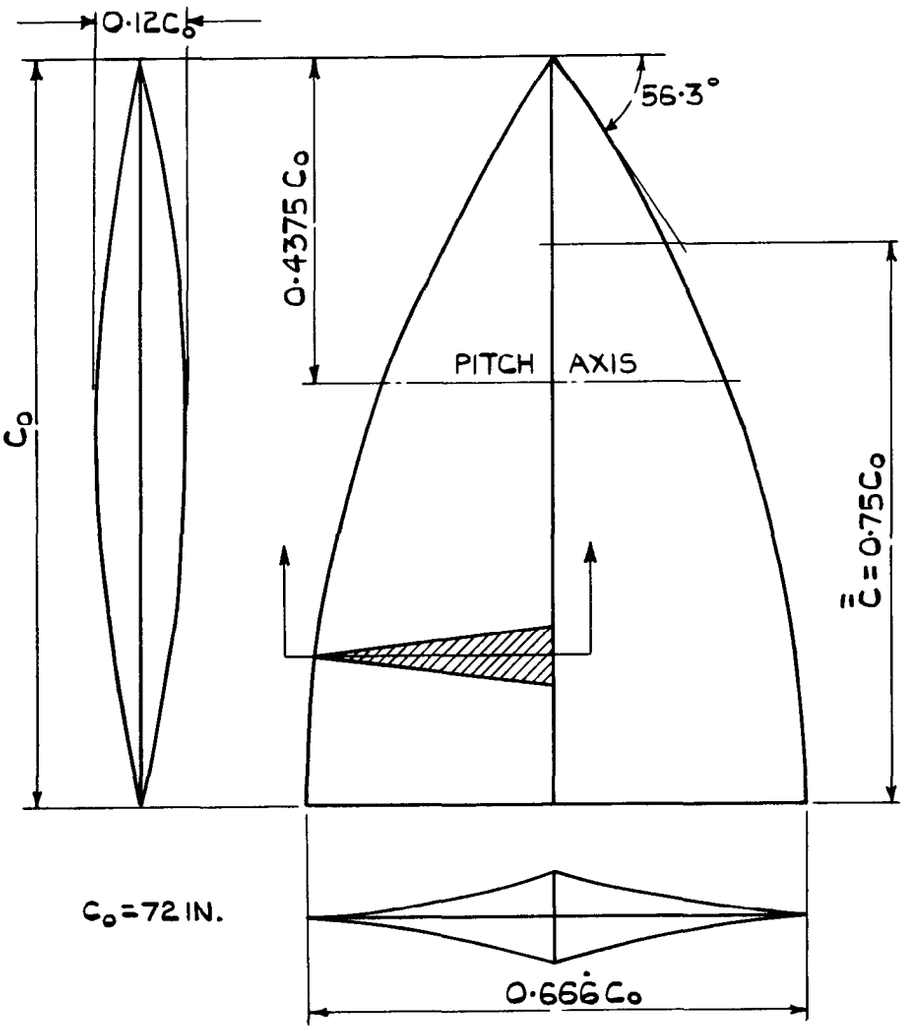


FIG. 2. WING GEOMETRY. A=1·0

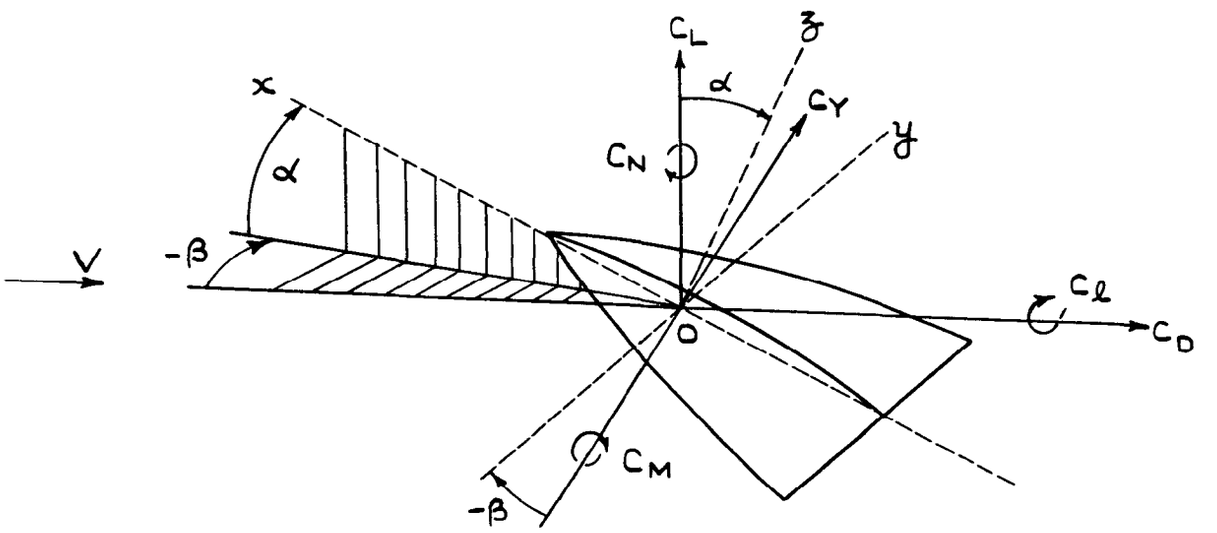


FIG. 3. FORCE AND MOMENT AXES.

xyz - BODY AXES.

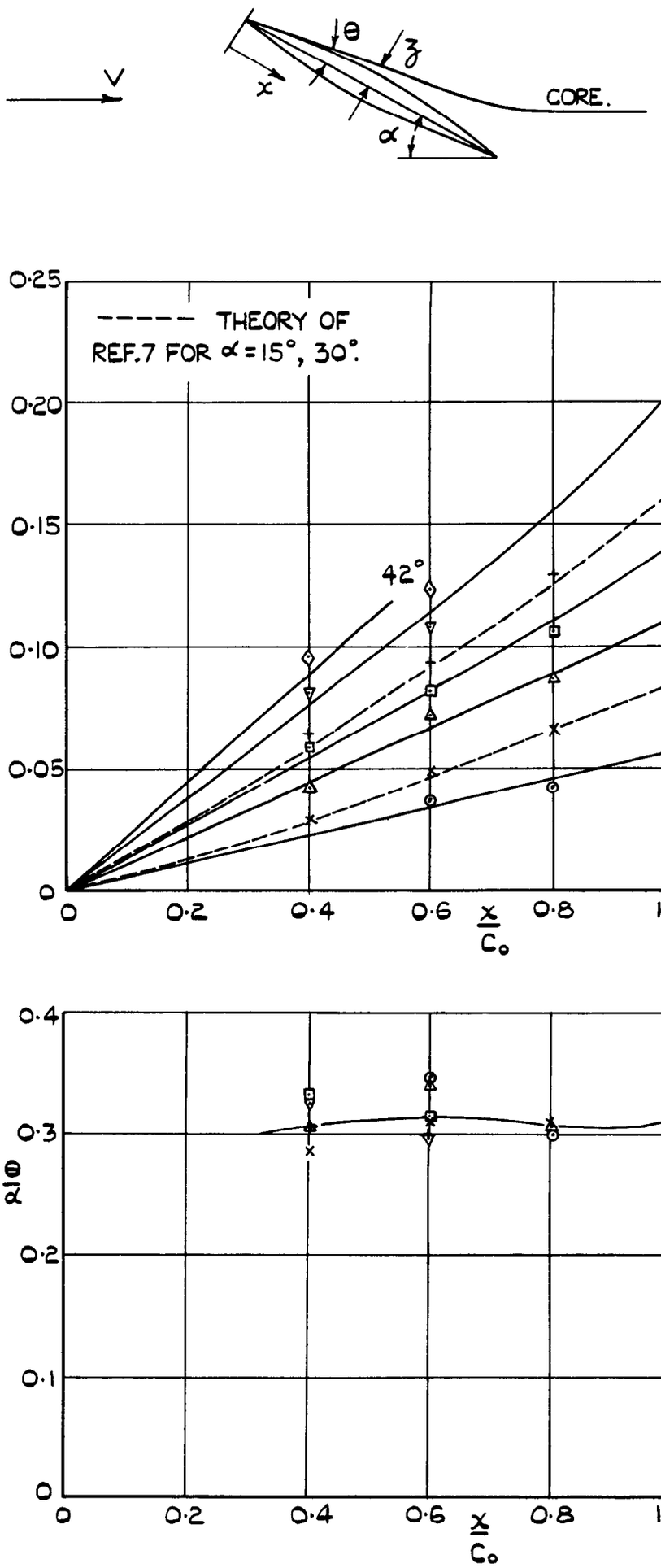


FIG. 4. SIDE ELEVATION OF VORTEX CORE PATH.

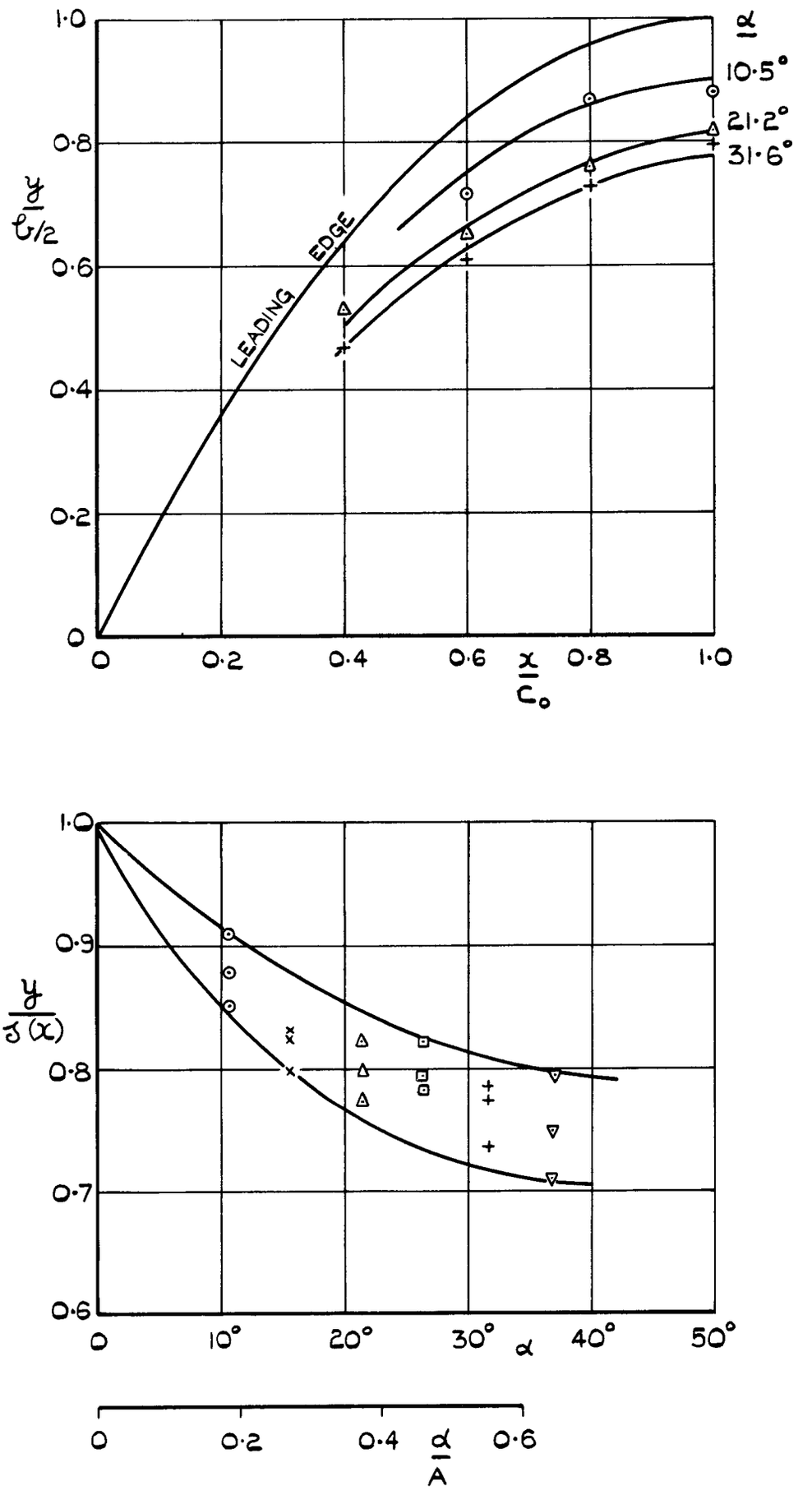


FIG.5. PLAN VIEW OF VORTEX CORE PATH.

$s(x)$ = LOCAL SEMI-SPAN.

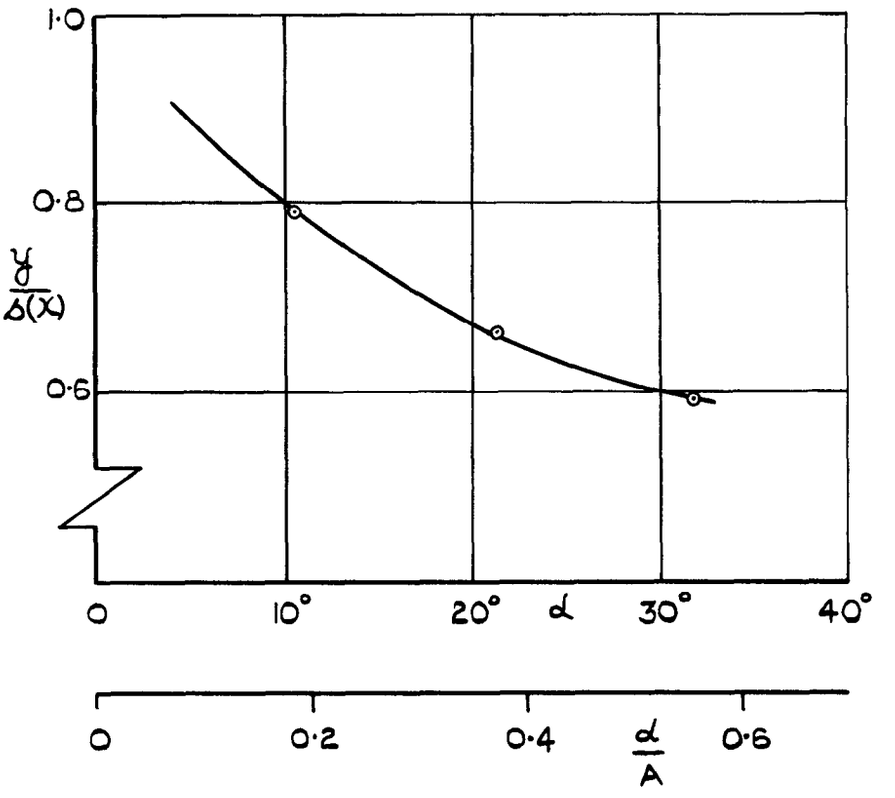


FIG. 6. SPANWISE POSITION OF THE POINT OF INFLECTION.

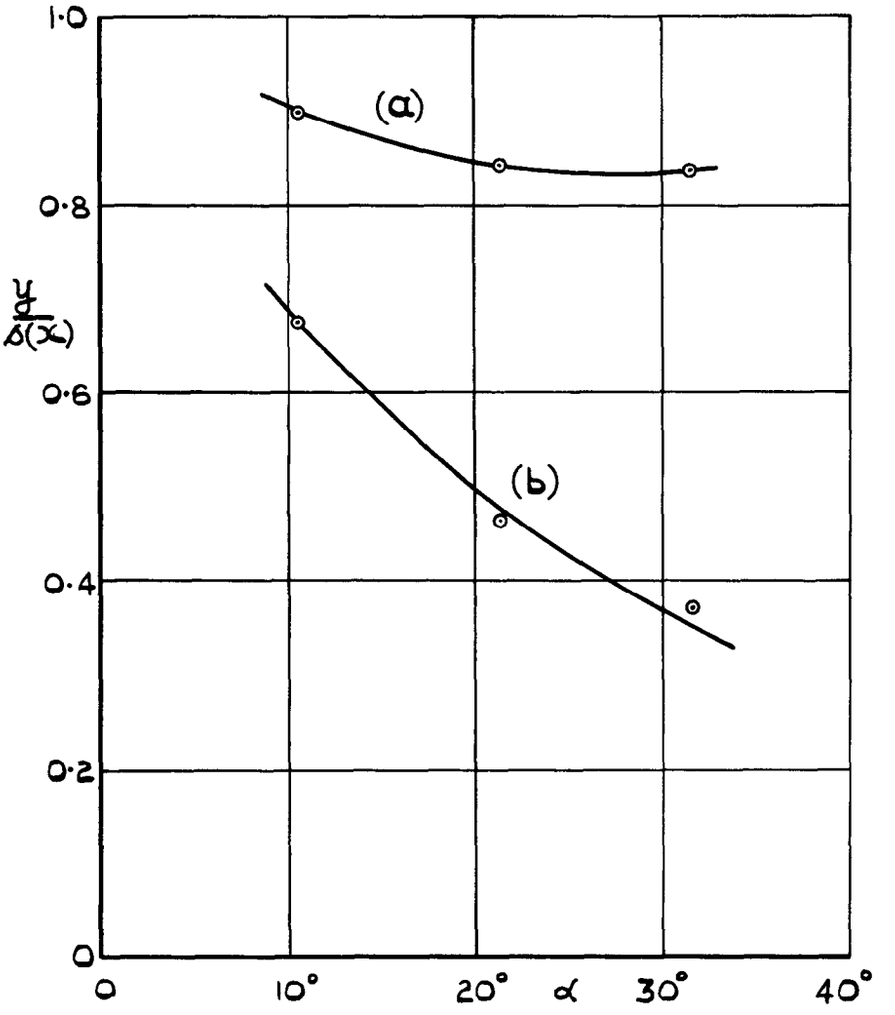


FIG. 7. POSITION OF THE SECONDARY SEPARATION (a) & THE ATTACHMENT LINE (b)

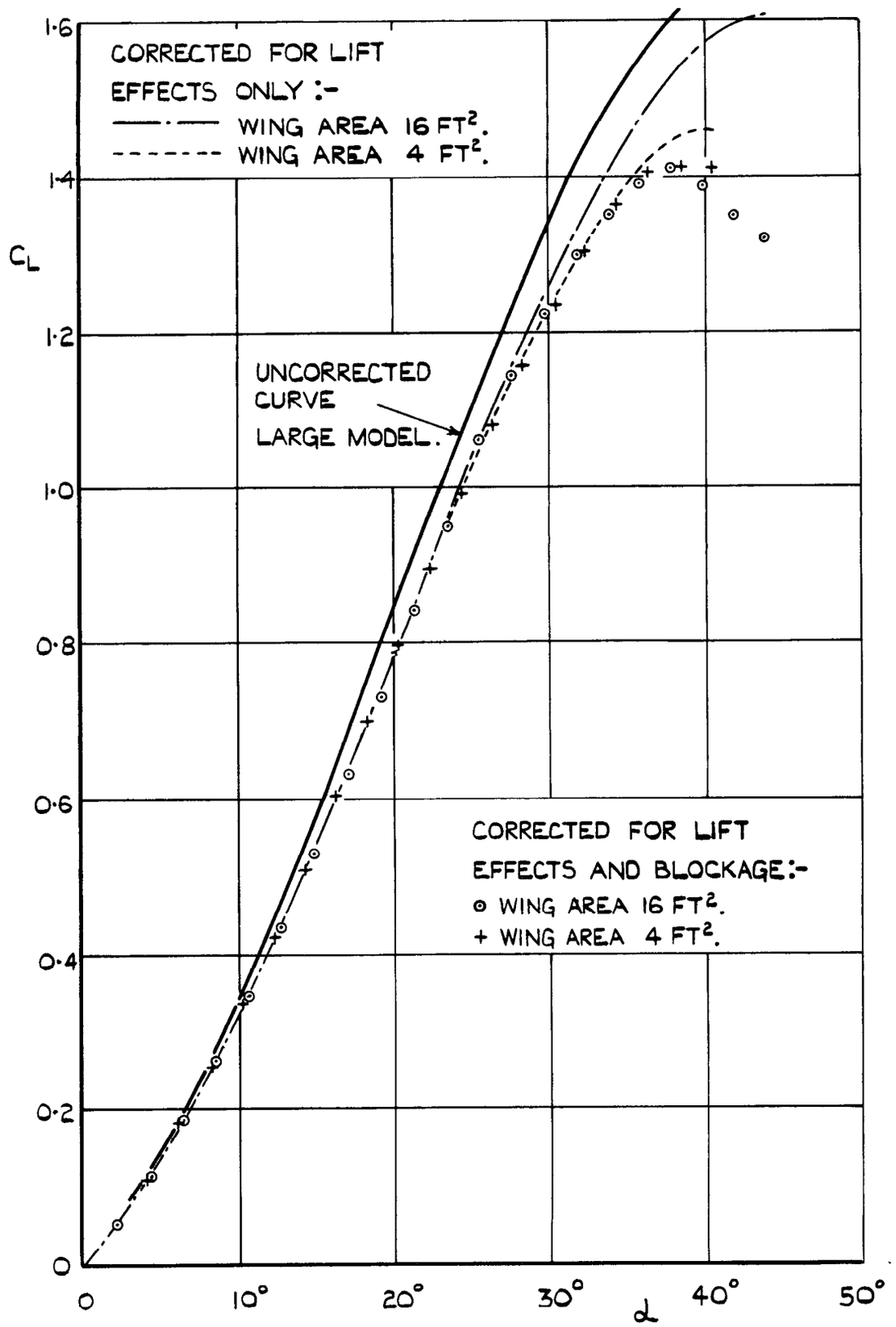


FIG. 8. EFFECT OF BLOCKAGE ON OVERALL LIFT COEFFICIENT OF A = 1·0 GOTHIC WING IN 13′ x 9′ TUNNEL.

WORKING SECTION C.S.A. = 111·4 FT².

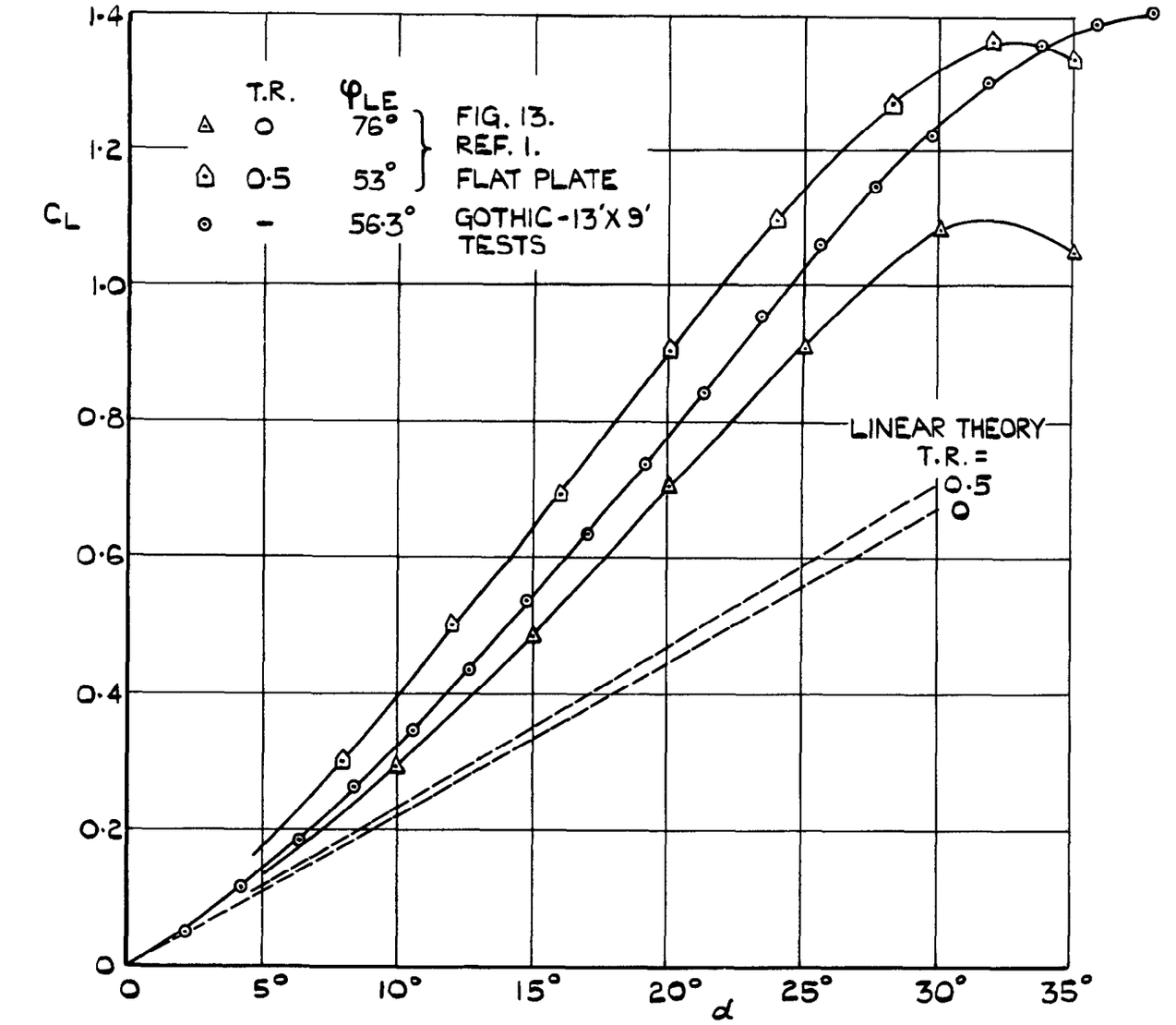


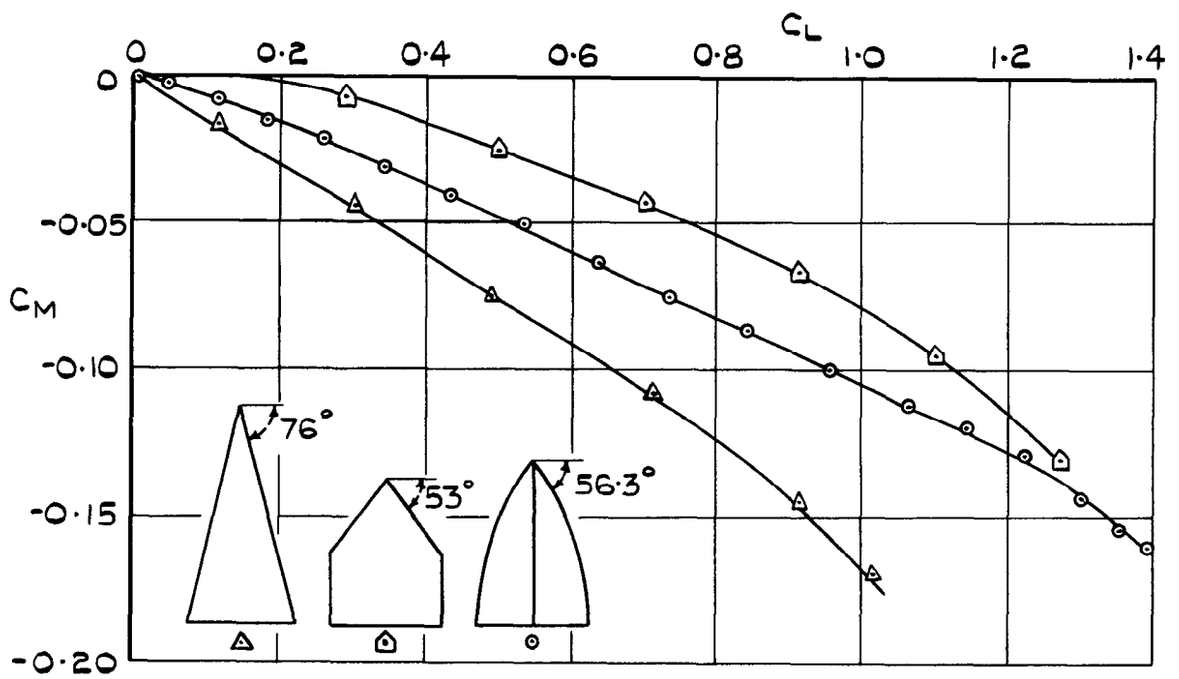


FIG. 9. EFFECT OF LEADING EDGE PLANFORM SHAPE ON LIFT AND PITCHING MOMENT OF WINGS OF ASPECT RATIO 1·0 WITH STRAIGHT TRAILING EDGES.

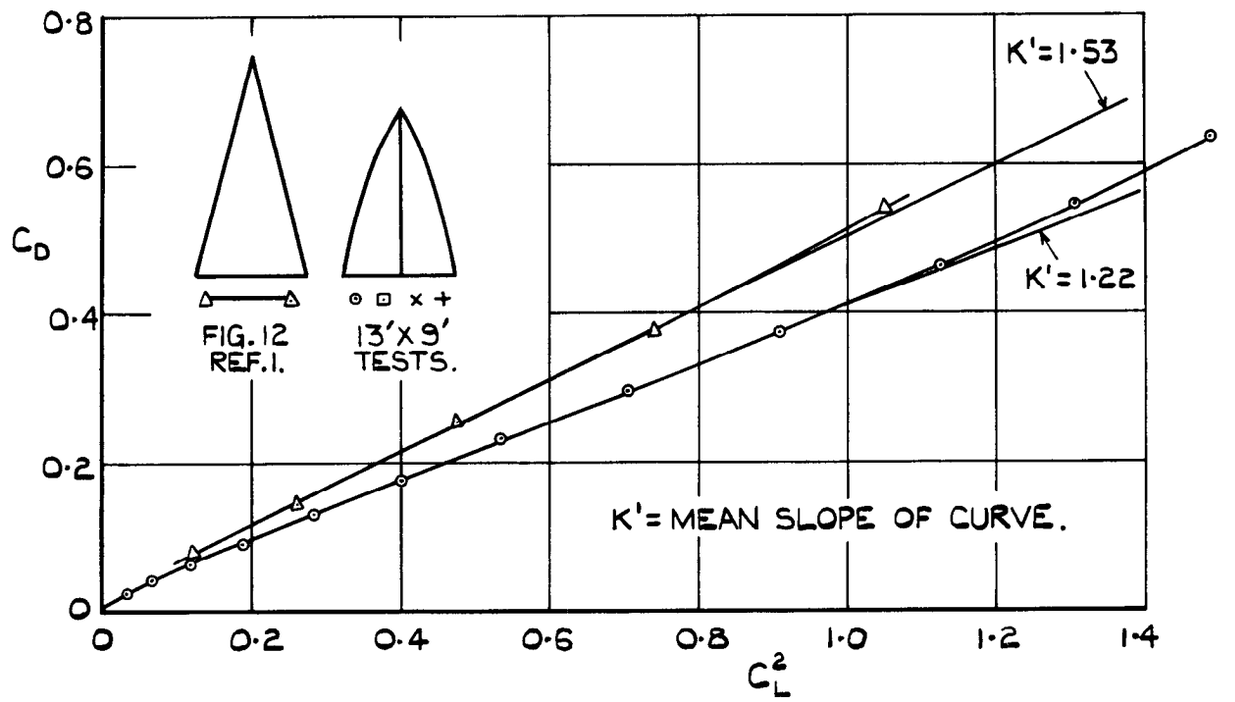


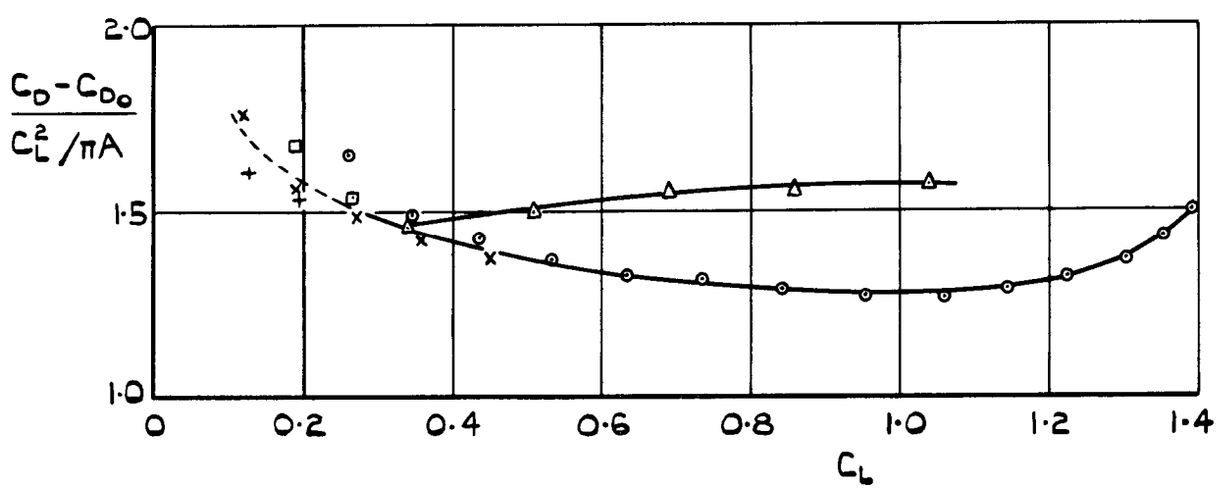


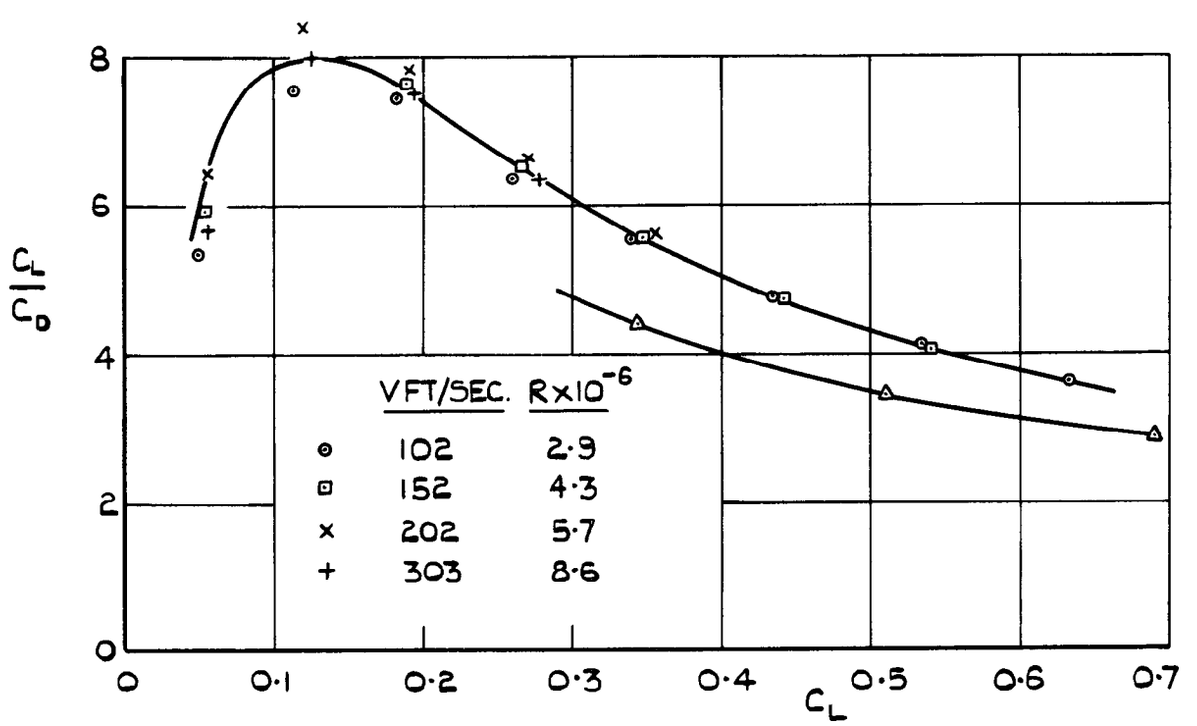


FIG. 10. DRAG CHARACTERISTICS OF GOTHIC WING COMPARED WITH DELTA. A=1·0.

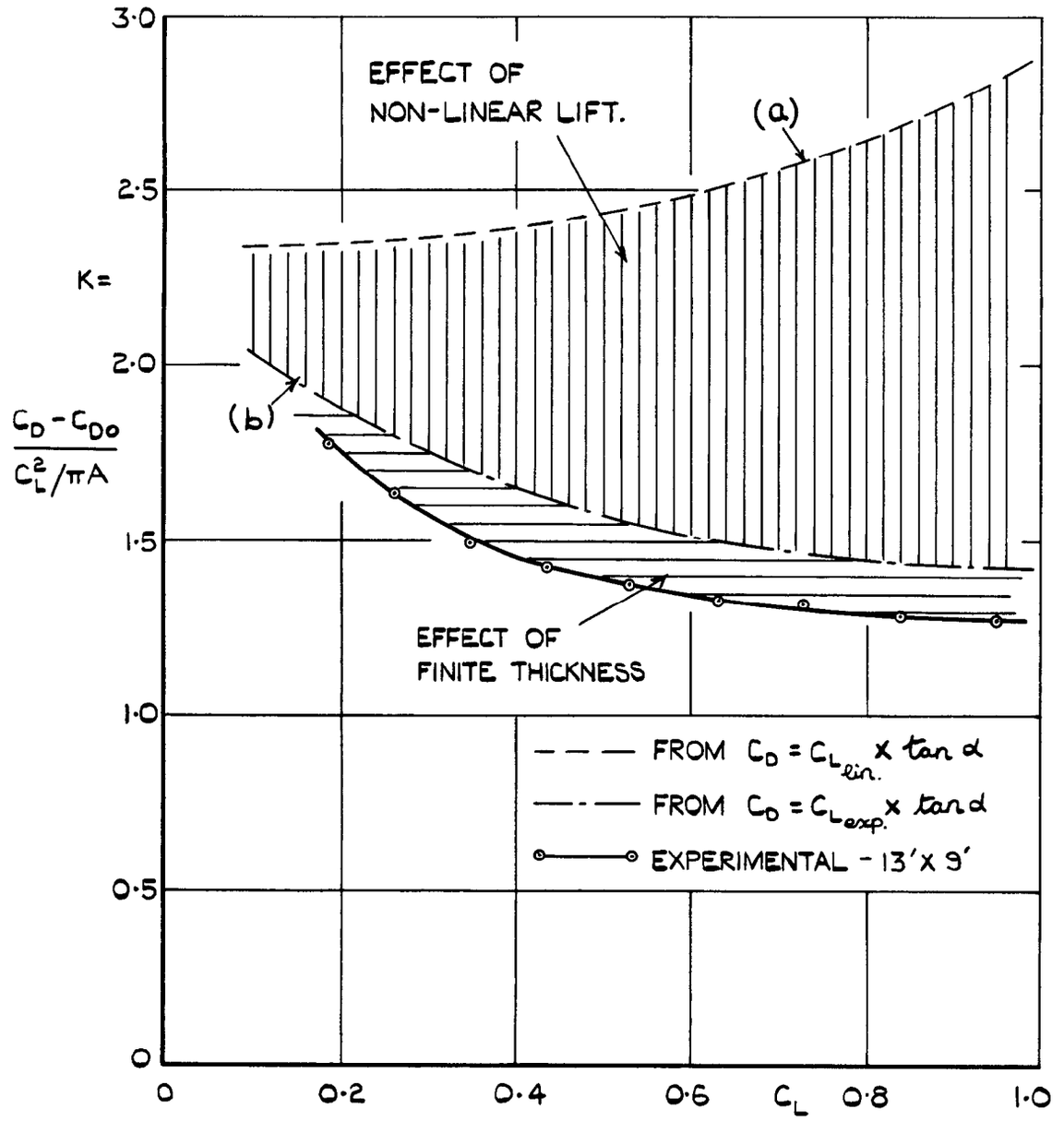


FIG.11. REDUCTION OF DRAG FACTOR DUE TO EFFECTS OF VORTEX SHEETS.

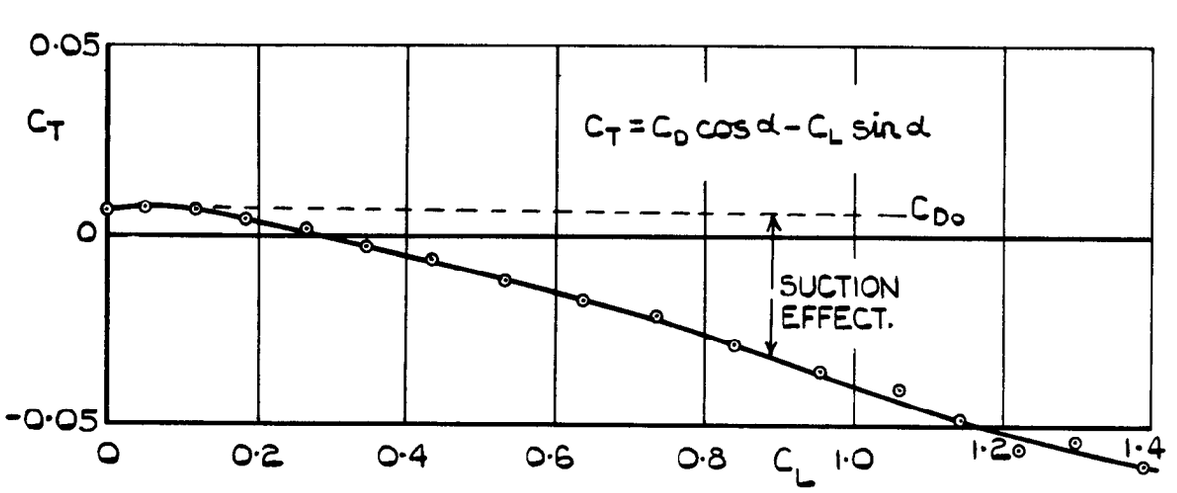


FIG.12. TANGENTIAL FORCE DUE TO SUCTION ON FORWARD FACING SURFACE.

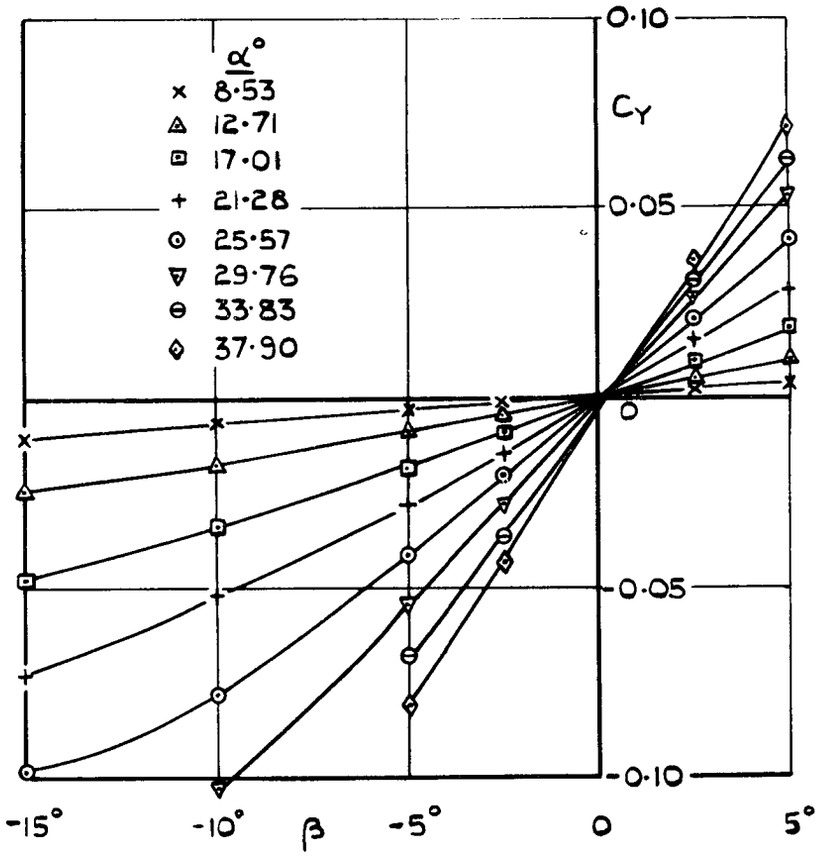


FIG.13. VARIATION OF SIDE FORCE COEFFICIENT WITH SIDESLIP.

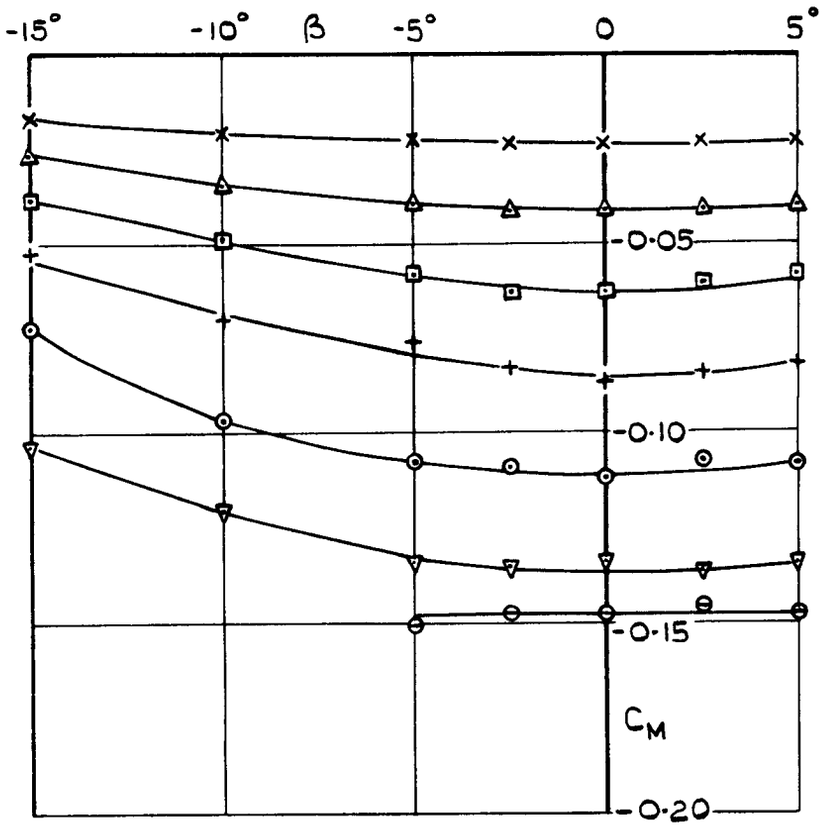


FIG.14. VARIATION OF PITCHING MOMENT COEFFICIENT WITH SIDESLIP.

(WIND AXES-ABOUT MEAN $\frac{1}{4}$ CHORD LINE)

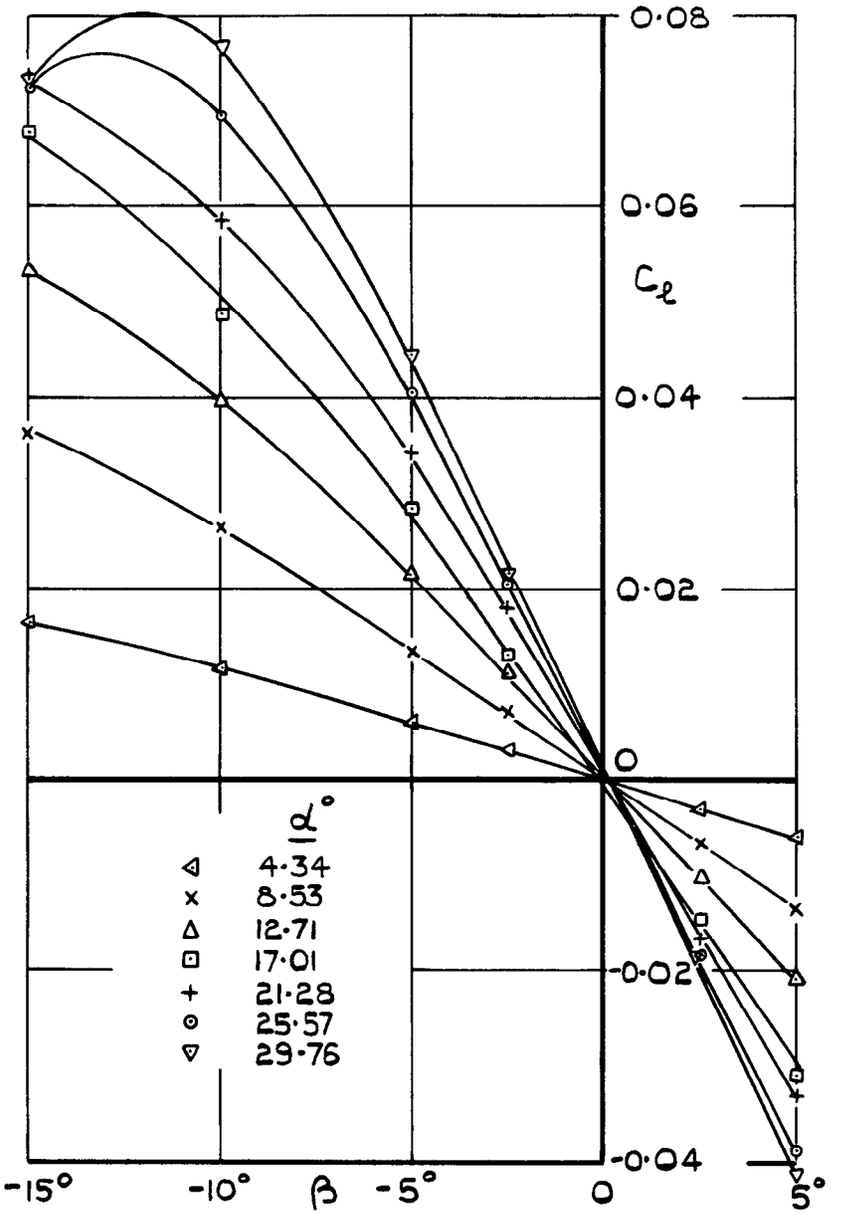


FIG.15. VARIATION OF ROLLING MOMENT COEFFICIENT WITH SIDESLIP (WIND AXES)

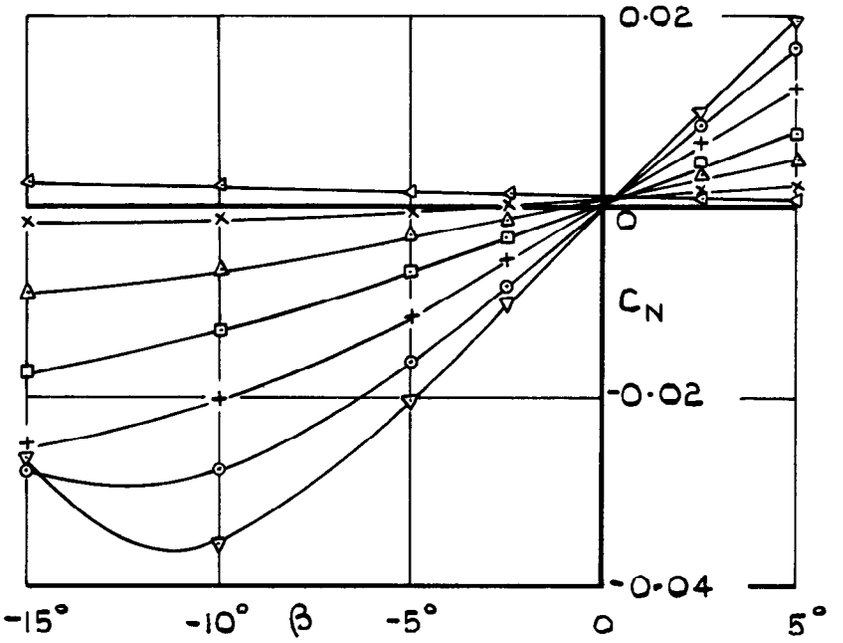


FIG.16. VARIATION OF YAWING MOMENT COEFFICIENT WITH SIDESLIP.
(WIND AXES — ABOUT MEAN $\frac{1}{4}$— CHORD POINT)

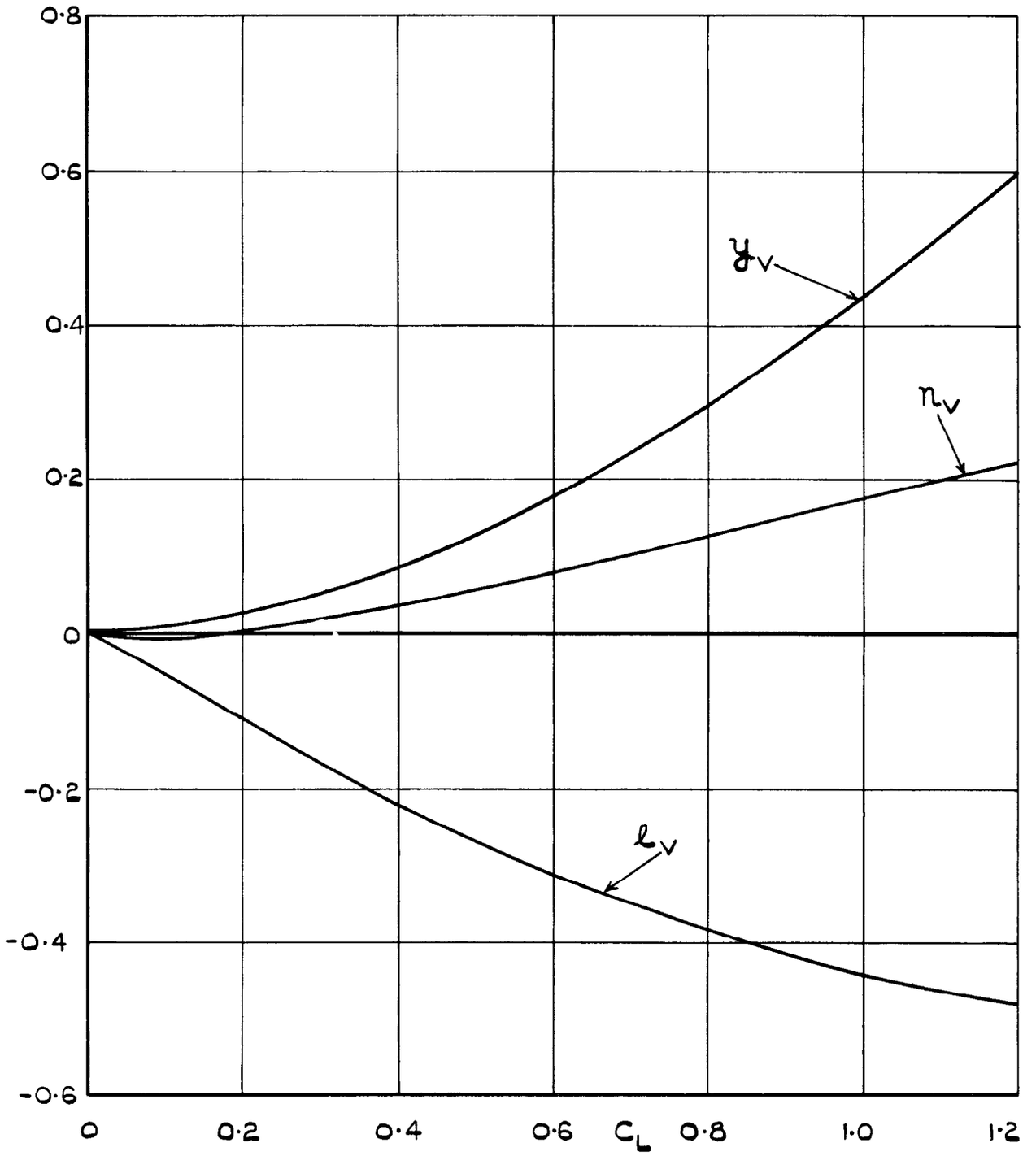


FIG. 17. LATERAL DERIVATIVES $y_v$, $\ell_v$, $n_v$.

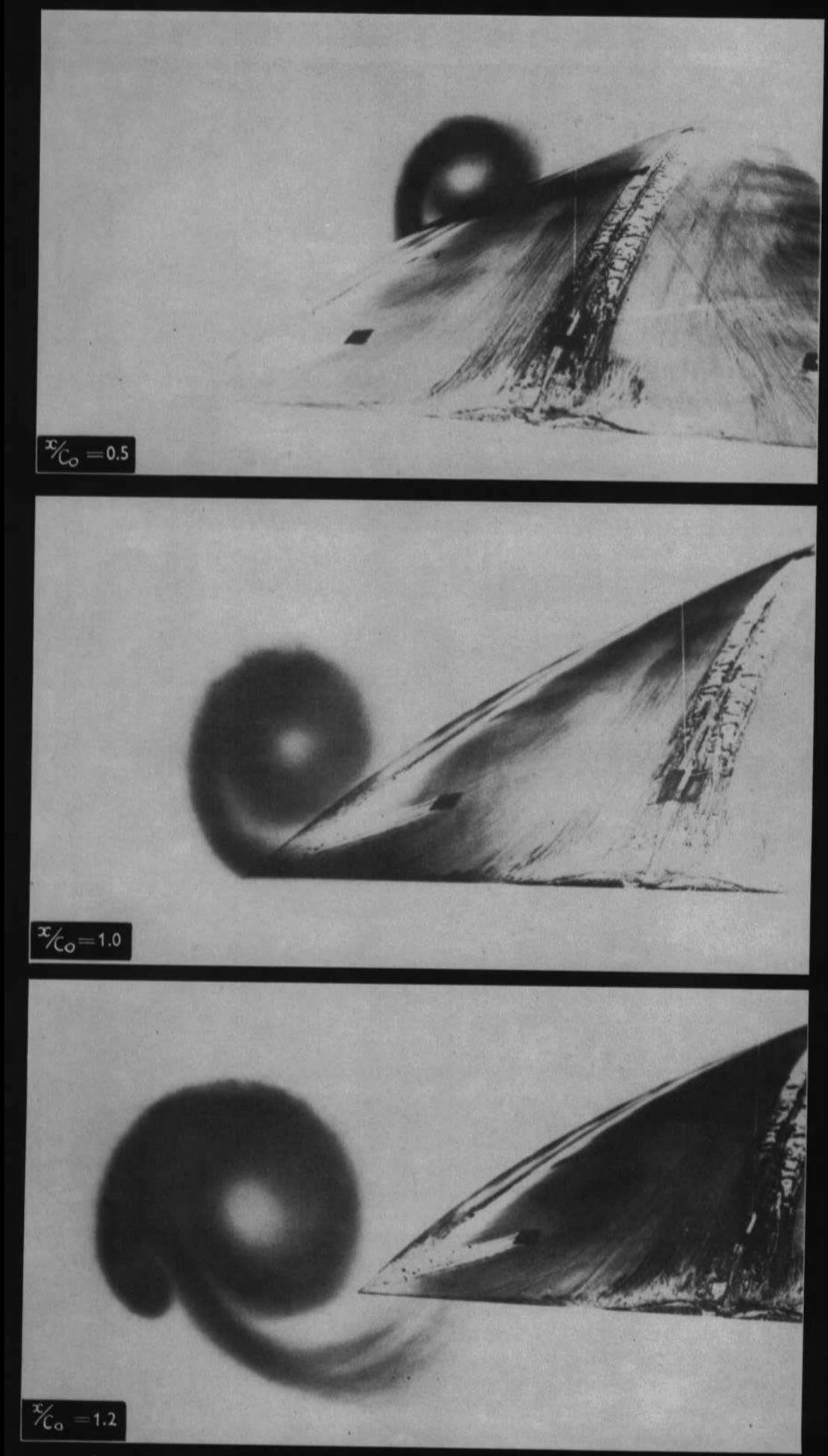


FIG. 18. DEVELOPMENT OF COILED VORTEX SHEETS FROM SHARP LEADING EDGE. $\alpha = 20°$

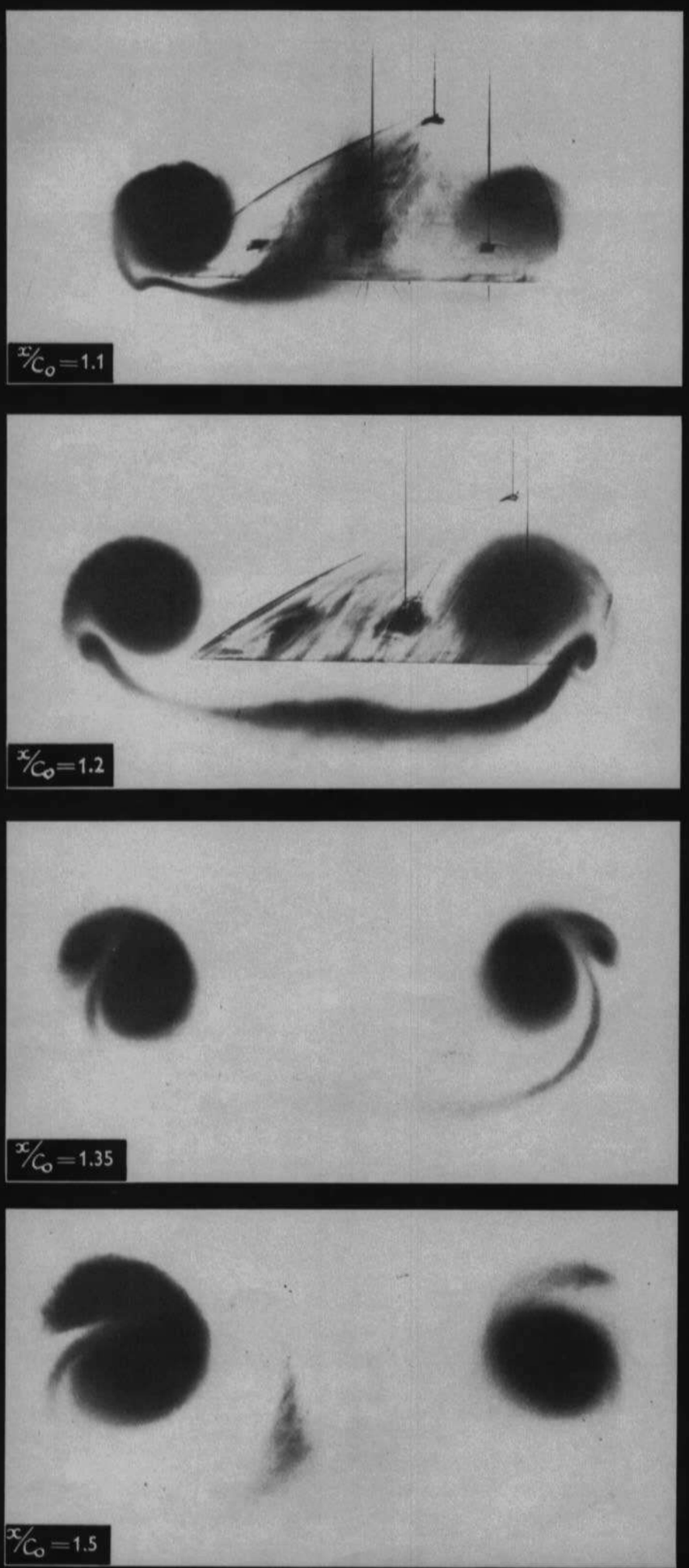


FIG.19. BEHAVIOUR OF COILED VORTEX SHEETS BEHIND WING. $\alpha = 20°$

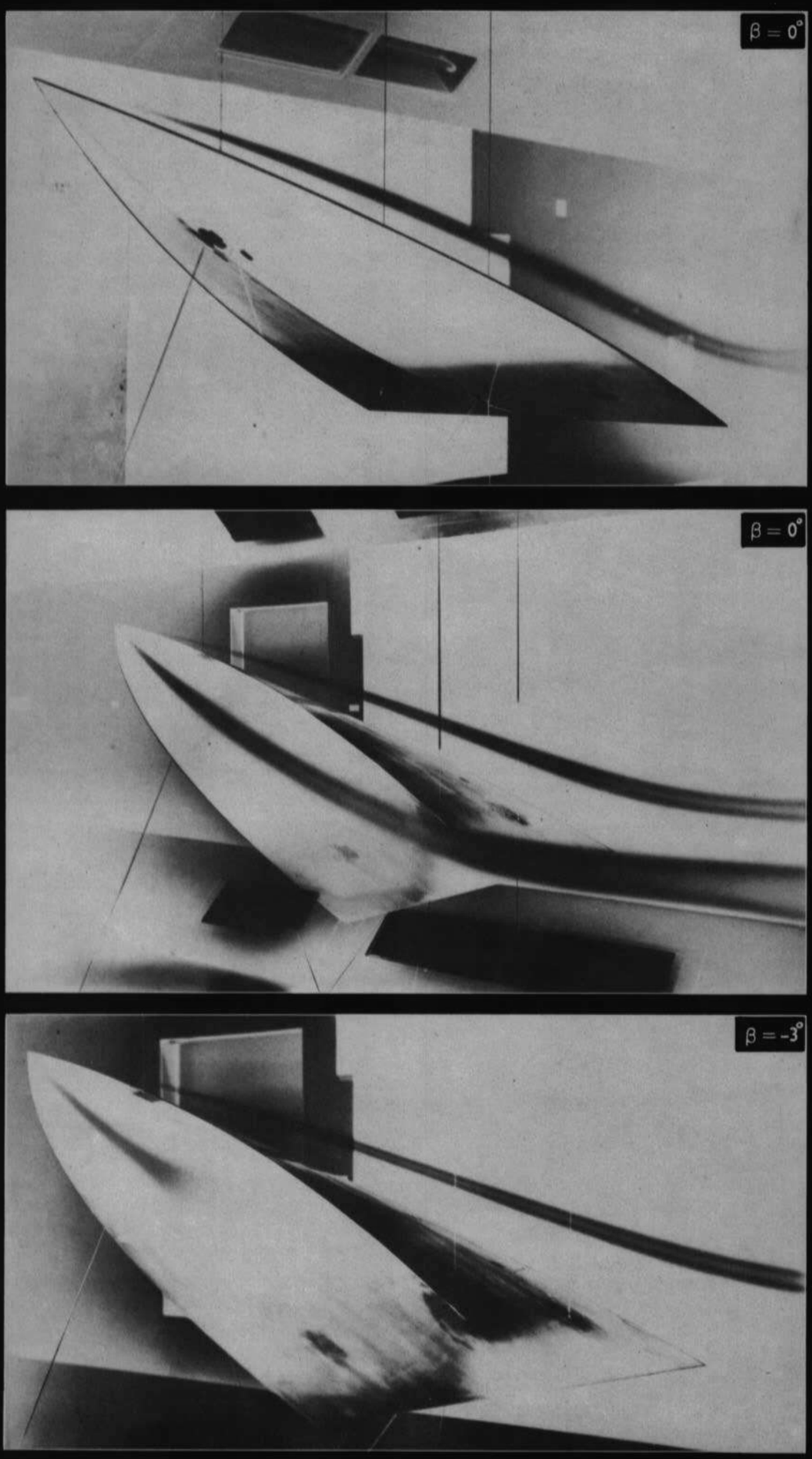


FIG.20. WATER VAPOUR CONDENSATION IN VORTEX SHEET CORES. $\alpha = 24°$

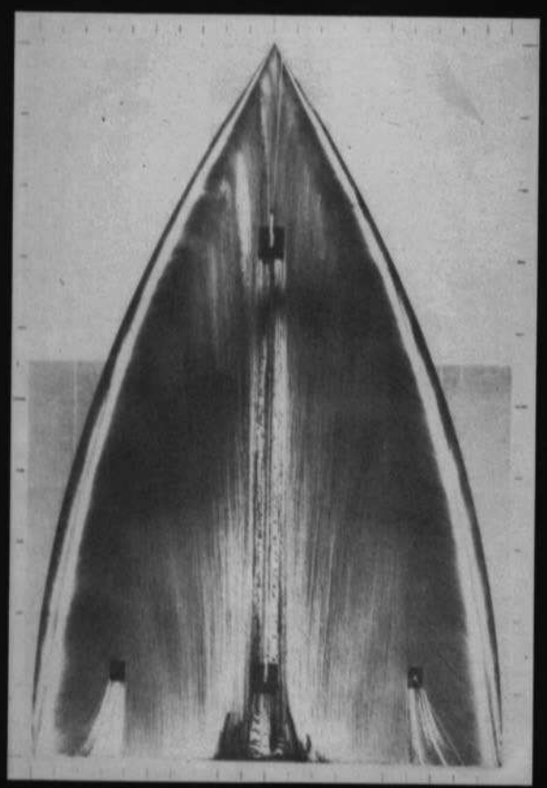

$\alpha = 10.5°$

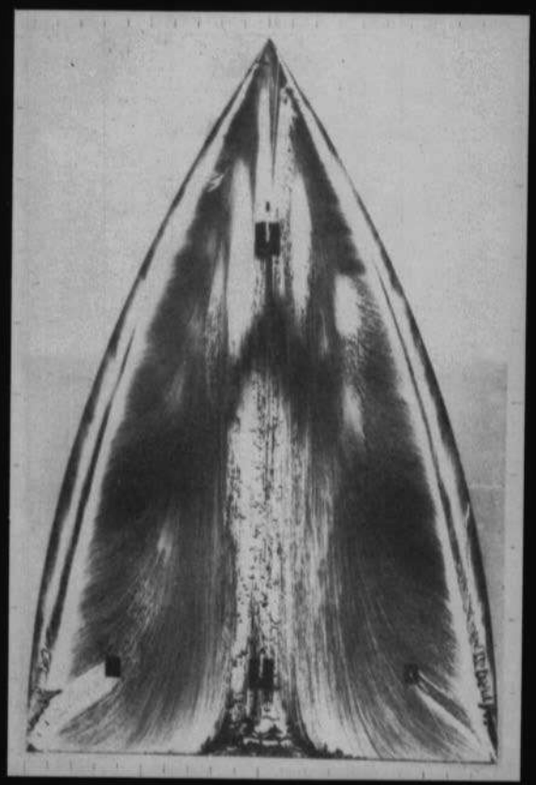

$\alpha = 21.2°$

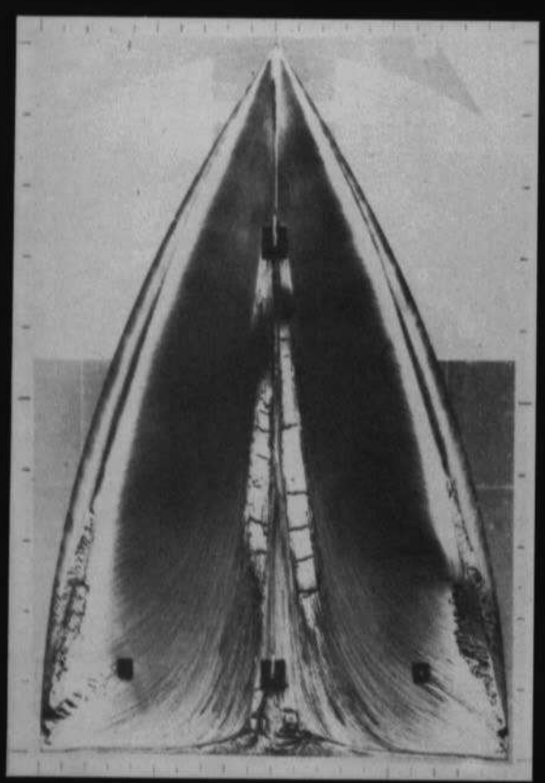

$\alpha = 31.6°$

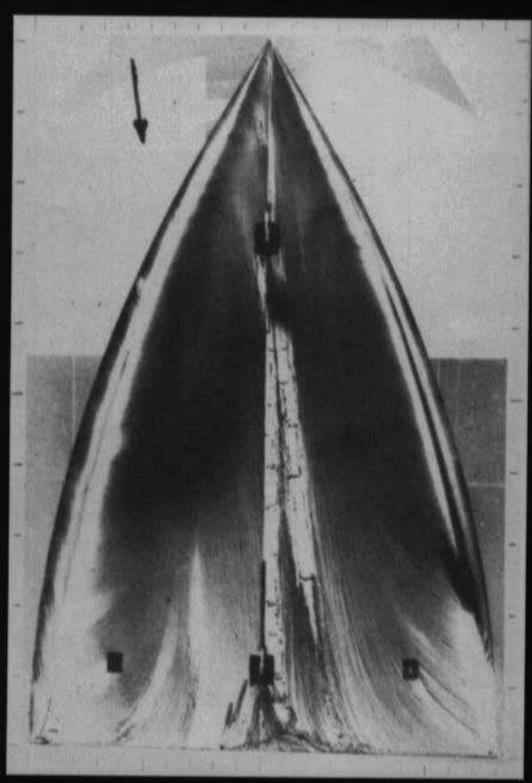

$\alpha = 21.2° \quad \beta = -5°$

FIG.21. VARIATION OF OIL FLOW PATTERNS WITH INCIDENCE AND YAW

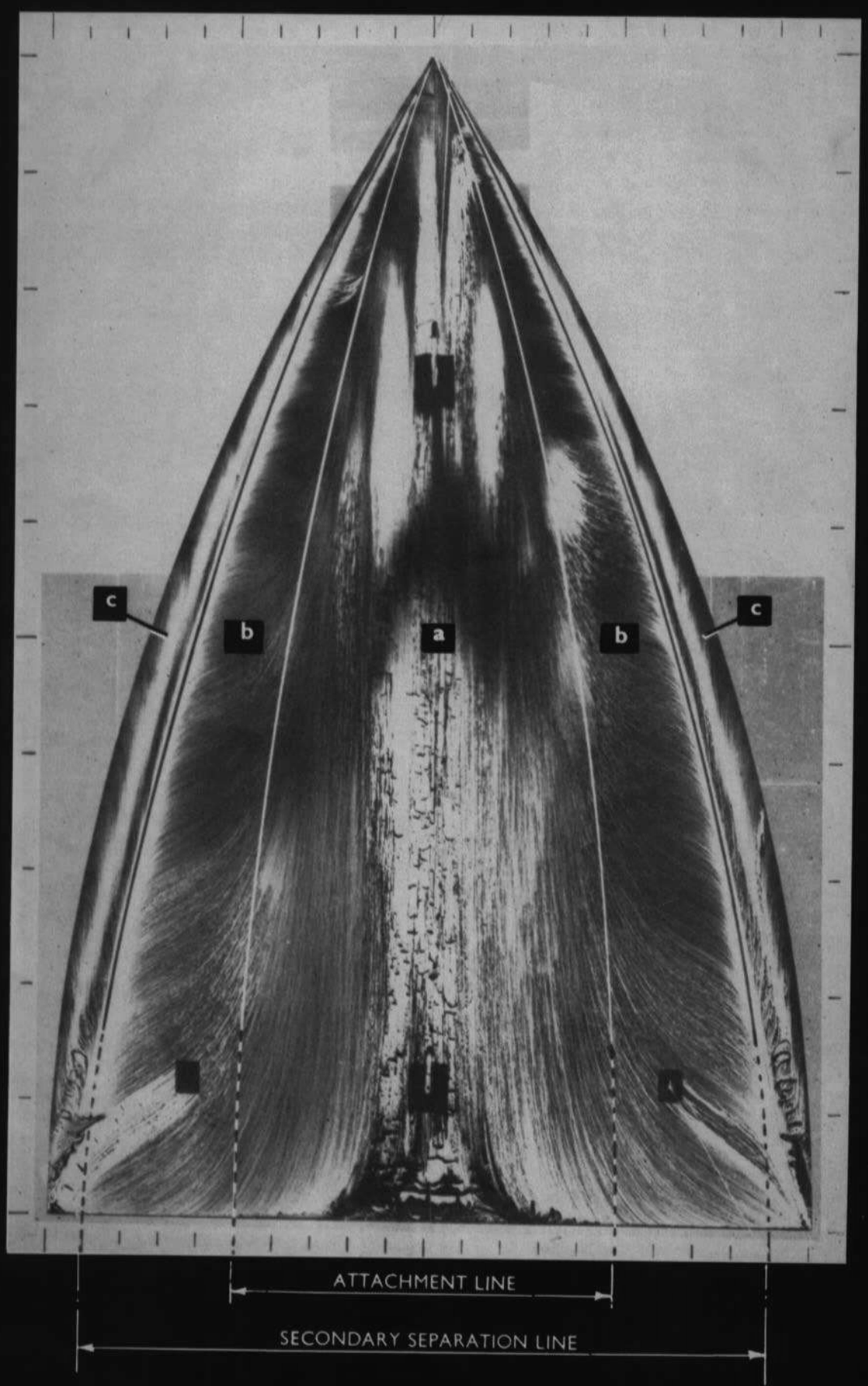


FIG.22. OIL FLOW PATTERN, $\alpha = 21.2°$

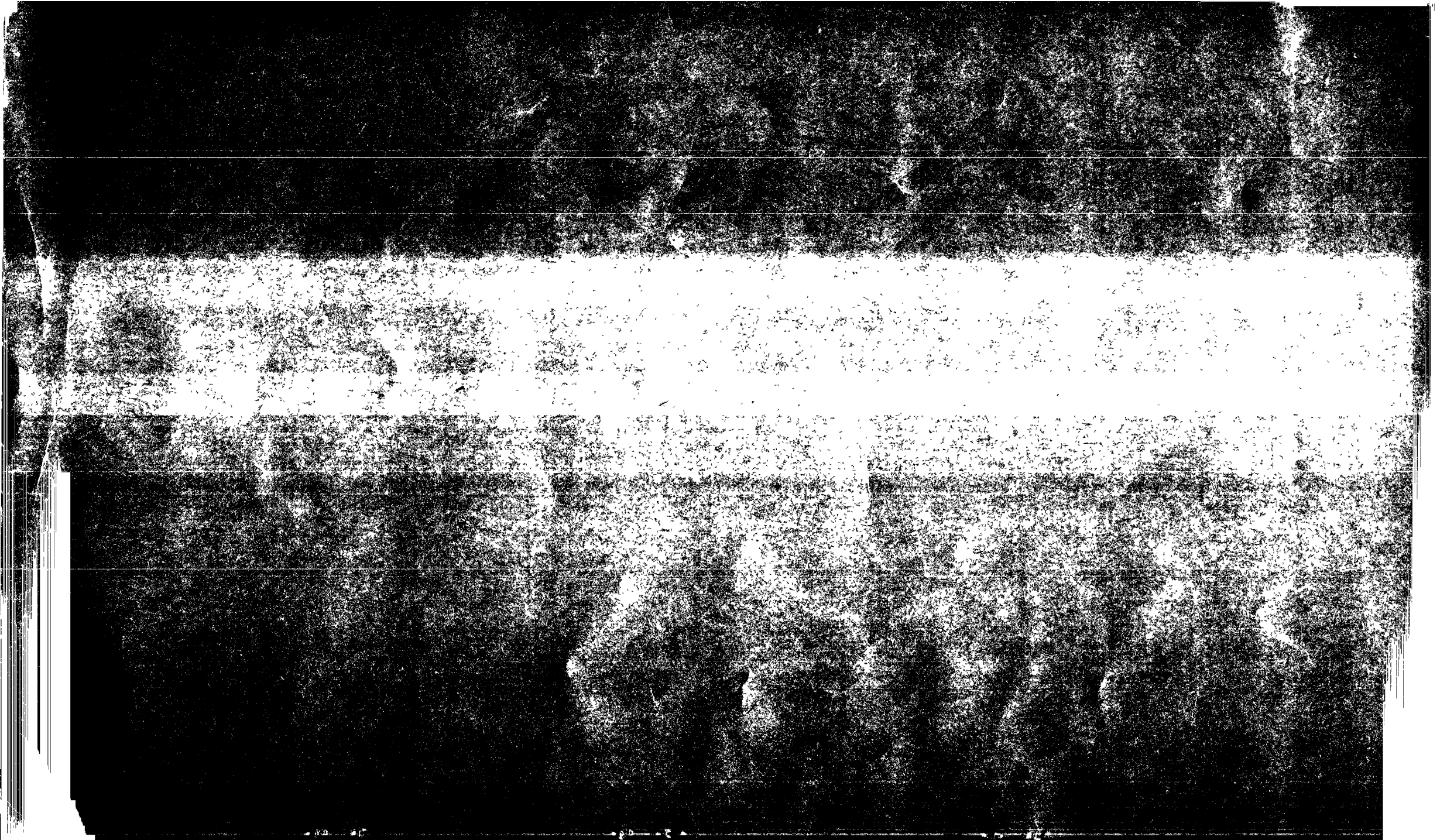

C.P. No. 508
(19,632)
A.R.C. Technical Report



Published by
HER MAJESTY'S STATIONERY OFFICE

To be purchased from
York House, Kingsway, London w.c.2
423 Oxford Street, London w.1
13A Castle Street, Edinburgh 2
109 St. Mary Street, Cardiff
39 King Street, Manchester 2
Tower Lane, Bristol 1
2 Edmund Street, Birmingham 3
80 Chichester Street, Belfast 1
or through any bookseller

*Printed in England*

S.O. Code No. 23-9012-8

C.P. No. 508